Accepted Manuscript

Design, synthesis and biological evaluation of 3-(imidazo[1,2-*a*]pyrazin-3-ylethynyl)-2-methylbenzamides as potent and selective pan-tropomyosin receptor kinase (TRK) inhibitors

Shenyang Cui, Yongjin Wang, Yuting Wang, Xia Tang, Xiaomei Ren, Lei Zhang, Yong Xu, Zhang Zhang, Zhimin Zhang, Xiaoyun Lu, Ke Ding

PII: S0223-5234(19)30591-4

DOI: https://doi.org/10.1016/j.ejmech.2019.06.064

Reference: EJMECH 11467

To appear in: *European Journal of Medicinal Chemistry*

Received Date: 21 February 2019

Revised Date: 21 June 2019

Accepted Date: 21 June 2019

Please cite this article as: S. Cui, Y. Wang, Y. Wang, X. Tang, X. Ren, L. Zhang, Y. Xu, Z. Zhang, Z. Zhang, X. Lu, K. Ding, Design, synthesis and biological evaluation of 3-(imidazo[1,2-*a*]pyrazin-3-ylethynyl)-2-methylbenzamides as potent and selective pan-tropomyosin receptor kinase (TRK) inhibitors, *European Journal of Medicinal Chemistry* (2019), doi: https://doi.org/10.1016/j.ejmech.2019.06.064.

GA

Design, Synthesis and Biological Evaluation of 3-(imidazo[1,2-a]pyrazin-3-ylethynyl)-2-methylbenzamides as Potent and Selective pan-Tropomyosin receptor kinase (TRK) Inhibitors

Shenyang Cui,[a,b#] Yongjin Wang,[c#] Yuting Wang,[c#] Xia Tang,[c] Xiaomei Ren,[c] Lei Zhang,[d] Yong Xu,[a,b] Zhang Zhang,[c*] Zhimin Zhang,[c*] Xiaoyun Lu,[c*] Ke Ding[c*]

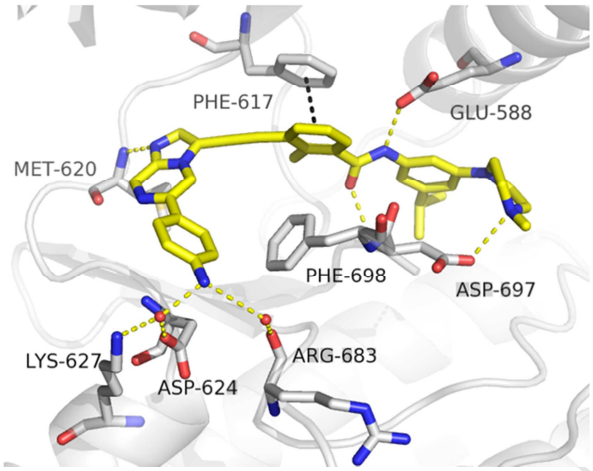

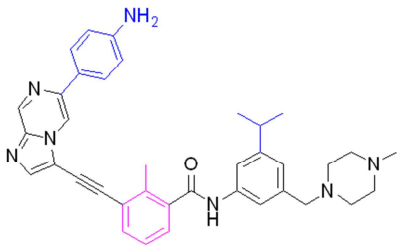

9o

IC_{50}: TRKA = 2.65 nM
TRKB = 10.47 nM
TRKC = 2.95 nM
Abl > 1 μM

A series of 3-(imidazo[1,2-a]pyrazin-3-ylethynyl)-2-methylbenzamides was designed and synthesized as new Trk inhibitors. **9o** suppressed TrkA/B/C with IC_{50} values of 2.65, 10.47 and 2.95 nM, respectively. **9o** also inhibited the proliferation of SH-SY5Y-TrkB cells with an IC_{50} value of 58 nM, and dose-dependently inhibited the BDNF-mediated TrkB activation and suppressed migration and invasion of SH-SY5Y-TrkB neuroblastoma.

Design, Synthesis and Biological Evaluation of 3-(Imidazo[1,2-a]pyrazin-3-ylethynyl)-2-methylbenzamides as New Tropomyosin receptor kinase (Trk) Inhibitors

Shenyang Cui,[a,b#] Yongjin Wang,[c#] Yuting Wang,[c#] Xia Tang,[c] Xiaomei Ren,[c] Lei Zhang,[d] Yong Xu,[a,b] Zhang Zhang,[c*] Zhimin Zhang,[c*] Xiaoyun Lu,[c*] Ke Ding[c*]

[a] Guangzhou Institutes of Biomedicine and Health, Chinese Academy of Sciences, No. 190 Kaiyuan Avenue, Guangzhou 510530, China

[b] University of Chinese Academy of Sciences, No. 19 Yuquan Road, Beijing 100049, China

[c] International Cooperative Laboratory of Traditional Chinese Medicine Modernization and Innovative Drug Development of Chinese Ministry of Education (MOE), Guangzhou City Key Laboratory of Precision Chemical Drug Development, School of pharmacy, Jinan University, No. 601 Huangpu Avenue West, Guangzhou 510632, China.

[d] National Facility for Protein Science in Shanghai, Zhangjiang Lab, Shanghai, 201210, China.

# These authors contributed equally.

[*]Corresponding authors: Tel: +86-20-85223764. E-mail: dingke@jnu.edu.cn.

Abstract

A series of 3-(imidazo[1,2-a]pyrazin-3-ylethynyl)-2-methylbenzamides was designed and synthesized as new tropomyosin receptor kinases (Trks) inhibitors by utilizing a structure-guided optimization strategy. One of the most potent compounds **9o** suppressed TrkA/B/C with IC_{50} values of 2.65, 10.47 and 2.95 nM, respectively. The compound dose-dependently inhibited brain-derived neurotrophic factor (BDNF)-mediated TrkB activation and suppressed migration and invasion of SH-SY5Y-TrkB neuroblastoma cells expressing high level of TrkB. Inhibitor **9o** also inhibited the proliferation of SH-SY5Y-TrkB cells with an IC_{50} value of 58 nM, which was comparable to that of a US FDA recently approved drug LOXO-101. Compound **9o** may serve as a new lead compound for further anti-cancer drug discovery.

Introduction

Tropomyosin receptor kinases (i.e. TrkA, TrkB and TrkC) are encoded by NTRK1, NTRK2 and NTRK3 genes, respectively, belong to the tyrosine receptor kinase superfamily. Trks are activated by neurotrophin family of growth factors including nerve growth factor (NGF), brain-derived neurotrophic

factor (BDNF), Neurotrophin-4 (NT-4) and Neurotrophin-3 (NT-3) [1]. Activation of Trks importantly affects differentiation, growth and survival of neurons. Particularly, Trks are pivotally involved in the synaptic strength and plasticity of the mammalian central system and peripheral nervous system [1-3]. Lack of Trks would result in incapacitation and deficiencies of neurons. For instance, the population of corneal sensory neurons is markedly depleted in TrkA (–/–) mice [4], animals lacking TrkB in parvalbumin-positive cells displayed sexually dimorphic behavioral phenotypes [5], while TrkC knockout mice exhibited profound deficiencies in CNS glial cells [6]. In tumor tissues, upon binding with the ligands, Trks are activated and downstream signals involving Ras/Erk, PI3K/Akt, and PLC-γ/PKC transduction pathways are triggered to stimulate cancer cell differentiation, proliferation, survival, angiogenesis, migration and metastasis [7, 8]. NTRKs gene fusion has been detected in multiple human cancers to express chimeric Trk proteins and leads to spontaneous ligand-independent dimerization and subsequent pathological activation of transduction pathways [7-9].

Neuroblastoma (NB) is one of most common and lethal solid tumors in children, for which less than 50% of patients classified as high-risk achieved long-term survival [10, 11]. Although TrkA and TrkC are commonly expressed in low-stage neuroblastomas, and are considered as predictive markers of a favorable outcome, TrkB and its ligand BDNF are highly expressed in more aggressive and fatal neuroblastomas [12, 13]. Collective investigations suggested that TrkB was heavily involved in proliferation and migration of NB cells and BDNF was able to enhance survival of TrkB-expressing neuroblastoma cell line SMS-KCM in serum-free media [12, 14-16]. TrkB expression in neuroblastomas is also associated with drug resistance and expression of angiogenic factors [17, 18]. Pan-Trk inhibitors, e.g. Entrectinib (**1**) and AZ623, had been demonstrated to strongly suppress BDNF-mediated proliferation of SH-SY5Y-TrkB neuroblastoma cells stably expressing high level of TrkB [15, 16]. Our previous investigation also showed that a novel Trk inhibitor GZD2202 effectively suppressed BDNF-mediated proliferation and metastasis in neuroblastoma models [19]. Moreover, studies also showed that TrkB contributes greatly to the poor prognosis of NB patients [8, 12]. These results collectively suggested Trks as highly promising molecular targets for new anti-NB drug discovery [8, 20].

A number of small molecule Trk inhibitors have been reported to date [20-23] (Figure 1). Among them, a type-I Trk inhibitor Larotrectinib (LOXO-101, **2**) was recently approved by U.S. Food and Drug Administration (FDA) for treatment of multiple cancers containing NTRKs fusions [24-26].

Entrectinib (**1**) represents another promising type-I Trk inhibitor which is currently in phase II clinical trials and has demonstrated robust therapeutic efficacy in patients with NTRKs, ROS1, and ALK fusions, regardless of cancer types [27-30]. Most recently, RIPMICF16 (**3**) and TRACK (**4**) were also reported as novel Type I Trk inhibitors [31, 32]. Several other type-II multi-target kinase inhibitors, e.g. cabozantinib (**5**), sitravatinib (**6**) and altiratinib (**7**), are also in different stages of clinical investigation for treatment of cancer patients with NTRKs fusions [33-36]. Nevertheless, most of the Trk inhibitors are still suffering from relatively low target specificity. Moreover, acquired drug resistance against the available Trk inhibitor drugs was reported [37, 38]. It is highly desirable to discover new selective Trk inhibitors with distinct chemical scaffolds as new potential anti-neuroblastoma (NB) drugs.

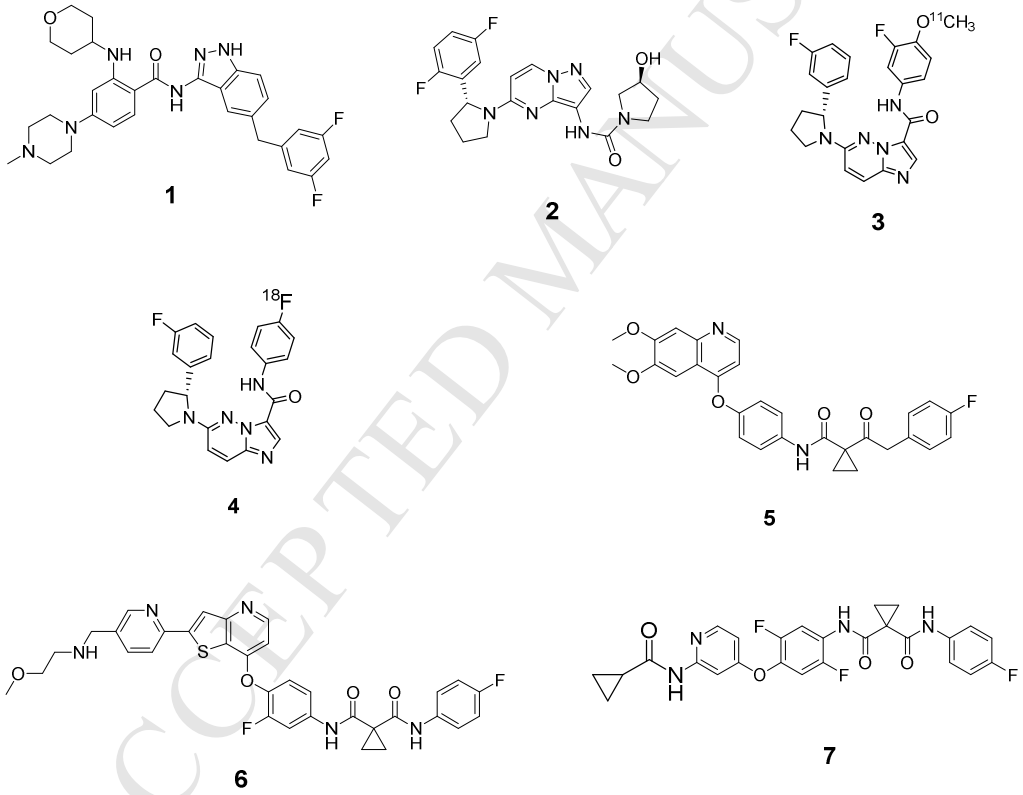

Figure 1. Chemical structures of representative Trk inhibitors.

3-(Imidazo[1,2-a]pyrazin-3-ylethynyl)-4-methyl-*N*-(3-((4-methylpiperazin-1-yl)methyl)-5-(trifluoro methyl)phenyl)benzamide (**8**) is a highly potent Abelson tyrosine kinase (Abl) inhibitor recently discovered in our laboratory [39]. Interestingly, this compound also exhibited strong suppressive effect against TrkA/B/C with IC_{50} values of 8.2, 9.4 and 4.4 nM, respectively. Aiming to eliminate the Abl inhibitory potency which may cause potential cardiotoxicity by inducing mitochondrial dysfunction [40,

41], a series of 3-(imidazo[1,2-a]pyrazin-3-ylethynyl)-2-methylbenzamide derivatives were designed and synthesized as new selective Trk inhibitors.

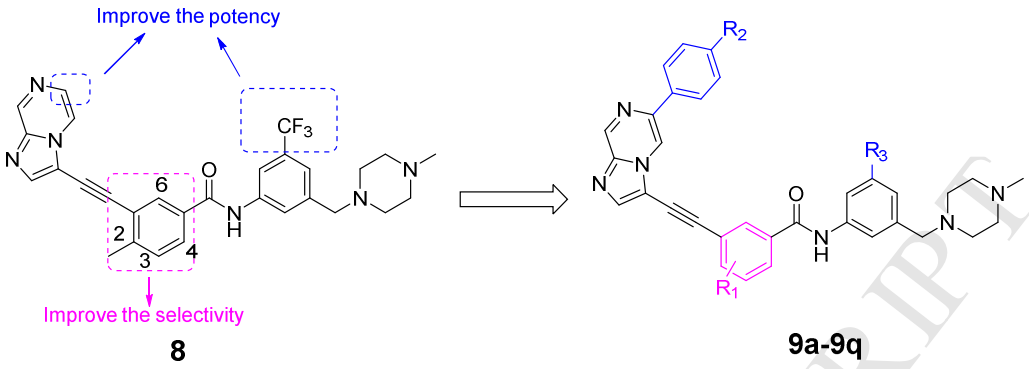

Figure 2. Structure-based optimization of 3-(imidazo[1,2-a]pyrazin-3-ylethynyl)-2-methylbenzamides as new selective Trk inhibitors.

Chemistry

The designed molecules were readily prepared using palladium-catalyzed Sonogashira coupling reactions [42] as the key steps (Scheme 1). Briefly, commercially available 3-bromobenzoic acid or 3-iodobenzoic acid (**10**) were treated with sulfurous dichloride in methanol to yield the methyl benzoates (**11**). The methyl benzoates (**11**) were reacted with excessive amounts of ethynyltrimethylsilane under palladium catalysis to afford the Sonogashira coupling products, which were further deprotected with K_2CO_3 to produce the terminal alkynes (**12**). The coupling of compounds **12** with commercially available or self-prepared heterocyclic bromides **13** (Scheme S1) under Sonogashira conditions afforded the intermediate methyl benzoates **14**. Methyl benzoates **14** were treated with 3-((4-methylpiperazin-1-yl)methyl)-5-(trifluoromethyl)aniline which were prepared based on the previously reported protocols [43] under basic conditions to produce designed inhibitors **9a-9i**, **9k** and **9l**. Intermediates **14** were hydrolyzed to generate benzoic acids **15**. The condensation of benzoic acids **15** with a series of substituted 3-((4-methylpiperazin-1-yl)methyl) anilines which were prepared based on the previously reported protocols [43] afforded the corresponding amides, which were further deprotected with trifluoroacetic acid to produce the designed inhibitors **9j, 9m-9q**.

Scheme 1. Syntheses of the designed molecules **9a-9q**. [a]

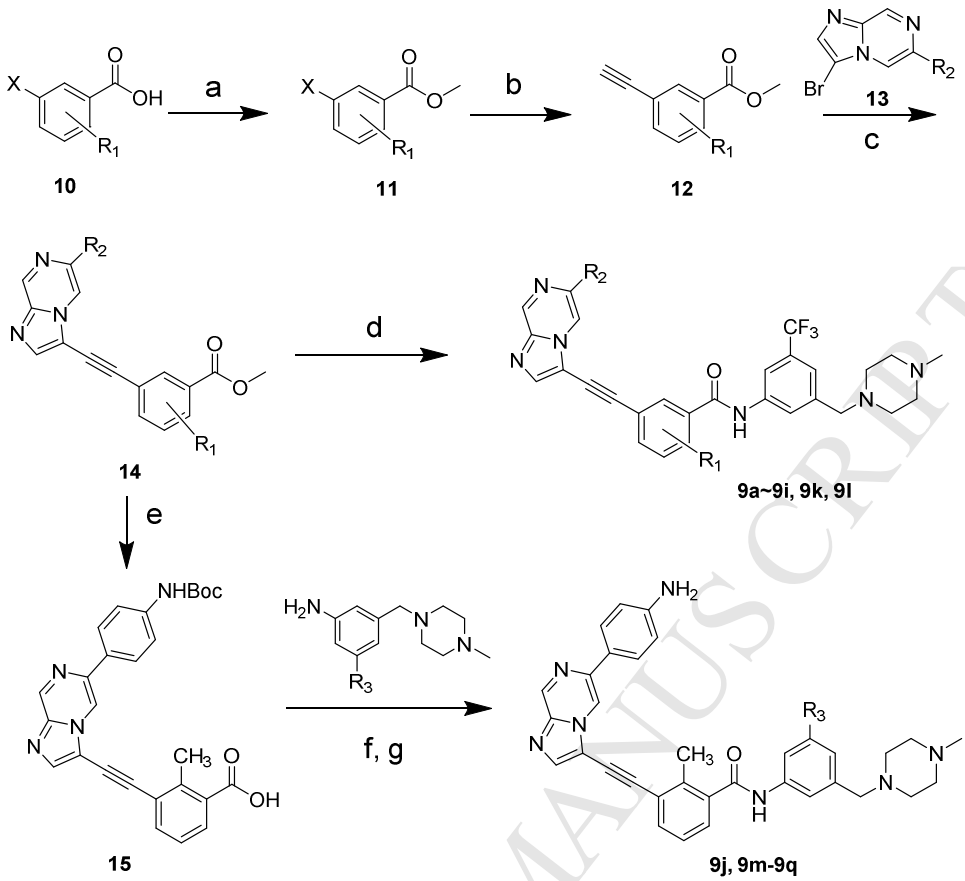

[a] **Reagents and conditions**: (a) sulfurous dichloride, methanol (MeOH), 60 □, 6 h, ~95%. (b) (i) trimethylsilyl acetylene, CuI, Bis(triphenylphosphine)palladium(II) chloride ($PdCl_2(PPh_3)_2$), triethylamine (Et_3N), acetonitrile (MeCN), 80 □, 12 h; (ii) K_2CO_3, MeOH, rt, 2 h, 50−92% (two steps). (c) CuI, $PdCl_2(PPh_3)_2$, *N*-ethyl-*N*-isopropylpropan-2-amine (DIPEA), *N*, *N*-dimethylformamide (DMF), 80 □, 18 h, 40~88%. (d) 3-((4-Methylpiperazin-1-yl)methyl) -5- (trifluoromethyl)aniline, potassium tert-butoxide (*t*-BuOK), tetrahydrofuran (THF), −20 °C to rt, 1 h, 40~70%. (e) Lithium hydroxide (LiOH), THF: H_2O = 2 : 1, rt, 4 h, 50%~70%. (f) 1-[Bis(dimethylamino)methylene]-1*H*-1, 2, 3 -triazolo[4,5-b]pyridinium 3-oxid hexafluorophosphate (HATU), DIPEA, DMF, rt, 6 h, 50~65%. (g) trifluoroacetic acid (CF_3COOH), dichloromethane (DCM), rt, 6 h, 80~90%.

Results and Discussion

Sequence analysis of TrkA/B/C and Abl kinase domains revealed that TrkA/B/C share 34%, 36% and 37% sequence identity with Abl in their kinase domains, respectively (Figure S1). A preliminary docking investigation suggested that **8** could bind with the inactive configurations of TrkA/B/C and Abl with similar type-II binding modes (data not shown). The investigation also suggested that the middle methylphenyl moiety of **8** adopted a different orientation in Trks (e.g. TrkC) comparing with it

in Abl (Figure 3A and 3B). This variation could be explained by the fact that methylphenyl moiety of **8** might form a potential π−π stacking interaction with Phe617 in TrkC, while the corresponding residue in Abl is Thr315 (Figure 3B). Investigation further implied that switching methyl group from 4'-position to other positions of the phenyl group could be a feasible strategy to improve the target selectivity against Trks over Abl. Based on this hypothesis, **9a**, **9b** and **9c**, in which a methyl was introduced at 5'-, 6'- or 2'- position of the corresponding phenyl moiety, respectively, were first designed and synthesized (Scheme 1). It was shown that the modification indeed significantly decreased inhibitory potencies against Abl (Table 1). However, the compounds also displayed obviously less Trks suppressive activities comparing to the lead molecule **8**. Significantly, 6'-methaylted molecule **9b** totally abolished inhibitory function against all of 3 isoforms of Trks. Although the 2'-methyl analogue **9c** exhibited 3~5-fold less potencies with IC_{50} values of 39.78, 38.35 and 11.46 nM, against TrkA, B and C, respectively, its inhibition against Abl decreased more than 500 folds. Further investigation also revealed that removal of 2'- methyl group in **9c** barely affected its potency against Trks (**9d**), but the modification obviously rescued Abl inhibition with an IC_{50} value of 33.31 nM. These data collectively suggested that 2'- position might be an optimal position for further structural modification to increase target selectivity of the compounds. However, structure activity relationship (SAR) exploration suggested that this position was not tolerated to a variety of substituents such as chloride (**9e**), methoxyl (**9f**), ethyl (**9g**), n-propyl (**9h**) and *i*-propyl (**9i**).

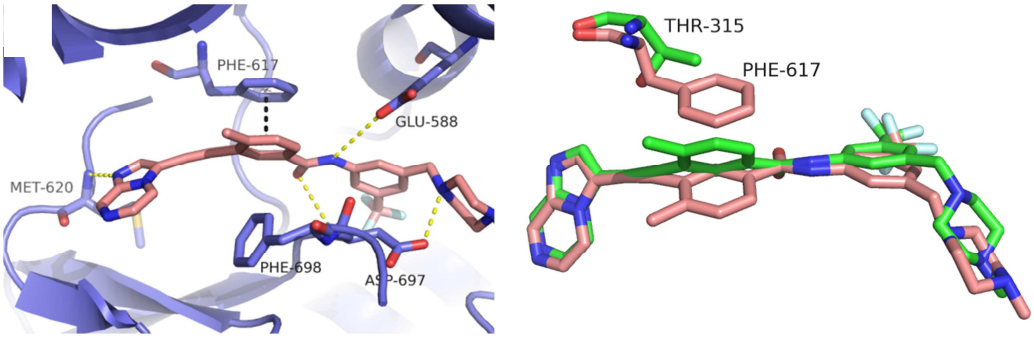

Figure 3. A) Docking studies of TrkC (PDB: 3V5Q) and compound **8**; the key residues of TrkC kinase is shown in blue stick and ribbon representation. Compound **8** is shown in orange stick structure. Hydrogen bonds are indicated by yellow dashed lines to key amino acids and π−π stacking interaction is indicated by black dashed lines. B) Superposition of the docking models of TrkC-**8** and Abl (PDB: 3OXZ) -**8** complexes. The residue thr315 and **8** in Abl are shown in green stick.

Table 1. *In vitro* inhibitory activities of compounds **9a**-**9i** against TrkA, TrkB, TrkC and Abl kinases. [a]

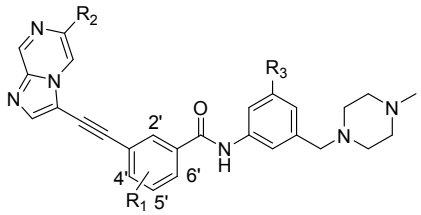

Compound	R1	R2	R3	TrkA	TrkB	TrkC	Abl
				IC_{50}(nM)			
8	CH_3(4'-)	H	CF_3	8.24±1.4	9.37±2.76	4.35±0.08	2.14±0.73
9a	CH_3(5'-)	H	CF_3	132.25±1.6	178.45±23.	66.98±20.9	449.1±56.9
9b	CH_3(6'-)	H	CF_3	>1μM	>1μM	934.9±261.	>1μM
9c	CH_3(2'-)	H	CF_3	39.78±8.2	38.35±9.3	11.46±1.03	>1μM
9d	H	H	CF_3	41.61±0.65	43.92±3.74	11.48±3.36	33.31±14.0
9e	Cl(2'-)	H	CF_3	226.55±34.	253.65±20.	44.58±5.31	>1μM
9f	OCH_3(2'-)	H	CF_3	>1μM	>1μM	692.5±229.	>1μM
9g	Et(2'-)	H	CF_3	186±18.82	315.13±6.0	129±27.35	>1μM
9h	n-Pr(2'-)	H	CF_3	>1μM	>1μM	>1μM	>1μM
9i	i-Pr(2'-)	H	CF_3	>1μM	>1μM	>1μM	>1μM
9j	CH_3(2'-)		CF_3	7.75±2.56	13.11±3.75	5.71±1.79	>1μM
9k	CH_3(2'-)		CF_3	29.2±6.25	22.73±8.69	16.8±10.52	>1μM
9l	CH_3(2'-)		CF_3	28.79±2.3	43.47±31.9	8.84±0.76	>1μM
9m	CH_3(2'-)		Me	17.43±3.97	41.34±19.9	14.55±5.52	>1μM
9n	CH_3(2'-)		Et	3.56±0.44	9.3±1.3	4.1±1.16	>1μM
9o	CH_3(2'-)		*i*-Pr	2.65±0.26	10.47±2.58	2.95±0.21	>1μM
9p	CH_3(2'-)		*t*-Bu	6.4±1.46	15.59±3.93	6.1±2.37	>1μM
9q	CH_3(2'-)		Ph	7.34±0.48	24.19±7.1	6.52±0.07	>1μM
LOXO-101				3.34±0.15	5.21±1.41	3.49±0.25	>1μM

[a] Trks and Abl activity experiments were performed using the FRET-based Z′-Lyte assay according to the manufacturer's instructions [44]. The data are mean values from at least three independent experiments.

We were able to solve a 2.0 Å X-ray co-crystal structure of **9c**-TrkC complex to elucidate the detail interaction of **9c** with Trks (Figure 4, Table S1). It was shown that **9c** fitted nicely into the ATP binding site of TrkC with a similar type-II binding mode to that was predicted (Figure 3A). The

imidazo[1,2-a]pyrazine moiety of **9c** formed an essential hydrogen bond with Met620 in the hinge region. Two additional hydrogen bonds were also formed between the amide and Glu588, and Asp697 from DFG-motif, respectively, while the methyl fitted nicely into a small hydrophobic pocket formed by the residues Val601, Leu686, and Phe698. In addition, the methylphenyl of **9c** indeed formed a π−π stacking interaction with Phe617.

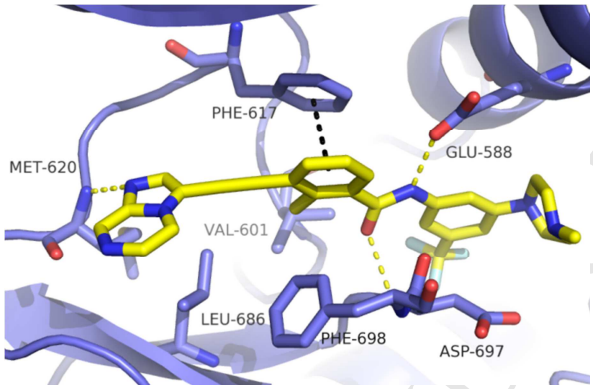

Figure 4. Co-crystal structure of TrkC and **9c** (PDB: ***). The key residues of TrkC kinase are shown in blue stick and ribbon representation. Compound **9c** is shown in yellow stick structure. Hydrogen bonds are indicated by yellow dashed lines to key amino acids and π−π stacking interaction is indicated by black dashed lines.

Analysis of TrkC-**9c** structure suggested that a polar recess formed by Asp624, Arg683, Leu686 and Phe698 could be accessible by the imidazo[1,2-a]pyrazine moiety of **9c** (Figure 5A). A hydrophilic substituent at R_2 might capture additional interaction with this pocket to achieve improved potency. Indeed, the 4-aniline substituted compound (**9j**) exhibited approximately a 3-fold improved potency with IC_{50} values of 7.75, 13.11 and 5.71 nM against TrkA, B and C, respectively, while the phenyl (**9k**) and pyridine (**9l**) derivatives were equally potent to **9c** (Table 1). Structural analysis also showed that the CF_3 group in **9c** bound deeply into a hydrophobic pocket formed by the DFG-out conformation. Consequently, SAR investigation was conducted to introduce various hydrophobic groups at R_3 position. It was found that this position was well tolerated to a variety of hydrophobic substituents with different sizes. Among all of molecules designed and synthesized, the *i*-Pr substituted derivative (**9o**) displayed the most potent inhibitory activities against TrkA, B and C with IC_{50} values of 2.65, 10.47 and 2.95 nM, respectively, which was equally potent to the US FDA recently approved drug LOXO-101.

A 1.7 Å resolution X-ray crystallographic structure of TrkC-**9o** complex was further determined to elucidate detail interactions between **9o** and Trks (Figure 5B, Table S1). It was shown that **9o** bound to TrkC with a similar type-II binding mode to that of **9c**. In accordance with the prediction, 4-aniline moiety indeed extended to the polar groove and the amino group formed hydrogen bonds network with Asp624, Lys627 and Arg683 mediated by waters (Figure 5B). Whereas, the *i*-Pr group fitted nicely into the hydrophobic pocket formed by the DFG-out conformation.

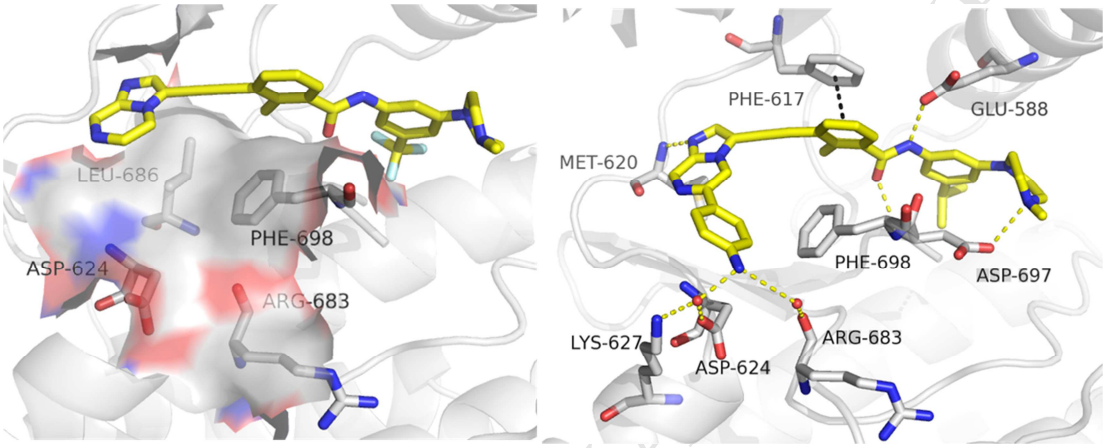

Figure 5. A) A small polar recess formed by Asp624, Arg683, Leu686 and phe698 in the crystal structure of TrkC-**9c**. The key residues of TrkC kinase are shown in gray stick and ribbon representation. Compound **9c** is shown in yellow stick structure. B) The crystal structure of TrkC and **9o** (PDB: ***). The key residues of TrkC kinase are shown in gray stick and ribbon representation. Compound **9o** is shown in yellow stick structure. Hydrogen bonds are indicated by yellow dashed lines to key amino acids and π−π stacking interaction is indicated by black dashed lines.

Inhibitory effects of compound **9o** on activation of TrkB and its downstream signals, e.g. Akt, Erk and PLC-γ, were also investigated in SH-SY5Y-TrkB cells stably expressing high level of TrkB (Figure 6). It was shown that **9o** dose-dependently inhibited the phosphorylation of TrkB and downstream signaling proteins Akt, Erk, PLC-γ. Substantial inhibition of TrkB activation by **9o** was observed at a concentration as low as 0.64 nM, and almost complete inhibition could be achieved at 16 nM or higher concentrations (Figure 6). However, no obvious effect was observed on Akt, Erk or PLC-γ signals by BDNF or **9o** in SH-SY5Y parental cells with low level of TrkB (Supporting Information). These data collectively suggested the selective inhibition of **9o** on the target.

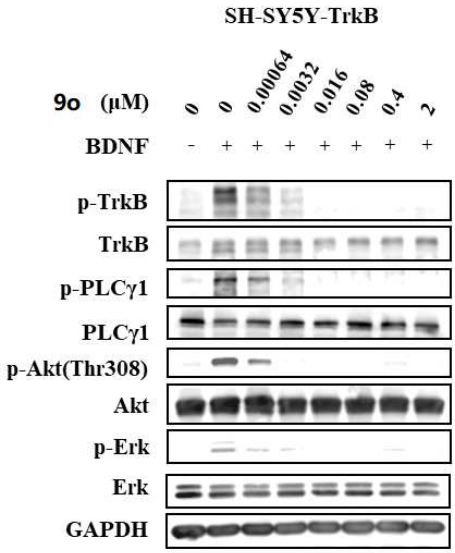

Figure 6. 9o inhibited TrkB activation induced by BDNF in SH-SY5Y-TrkB cells. SH-SY5Y-TrkB cells were pretreated with 0 to 2.0 μmol/L of **9o** for 6 h followed by BDNF (10 ng/mL) treatment for 30 min or not, then harvested and lysed. Cell lysates were separated by sodium dodecyl sulfate-polyacrylamide gel electrophoresis (SDS-PAGE) and analysed by Western blot for phosphorylated TrkB, TrkB, phosphorylated PLC-γ1, PLC-γ1, phosphorylated Akt (Ser473, Thr308), Akt, phosphorylated Erk and Erk. GAPDH was used as a control.

The migration inhibitory effect of **9o** on SH-SY5Y-TrkB neuroblastoma cells was initially investigated with a well-established wound healing assay [45]. It was shown that treatment of **9o** effectively inhibited migrating process in SH-SY5Y-TrkB cells, suppressing wound closure induced by BDNF (10 ng/mL) by 50.1%, 76.6% and 77.5% at concentrations of 8, 40 and 200 nM, respectively, compared to the untreated control (Figure 7A and 7B). Migration and invasion inhibitory potency of **9o** against SH-SY5Y-TrkB neuroblastoma cells was further validated by a standard transwell assay, which showed that **9o** dose-dependently inhibited migration and invasiveness of SH-SY5Y-TrkB neuroblastoma cells. Treatment with **9o** at 8, 40 or 200 nM for 24 h inhibited cancer cell migration by 22.7%, 53.3%, 82.0%; and inhibited invasion by 9.1%, 61.9% and 85.5% respectively ($p < 0.05$), compared to the BDNF (10 ng/mL) treatment; (Figure 7C and 7D). Collectively, these results suggest the promising potential of **9o** to produce an anti-metastasis effect in SH-SY5Y-TrkB neuroblastoma cells.

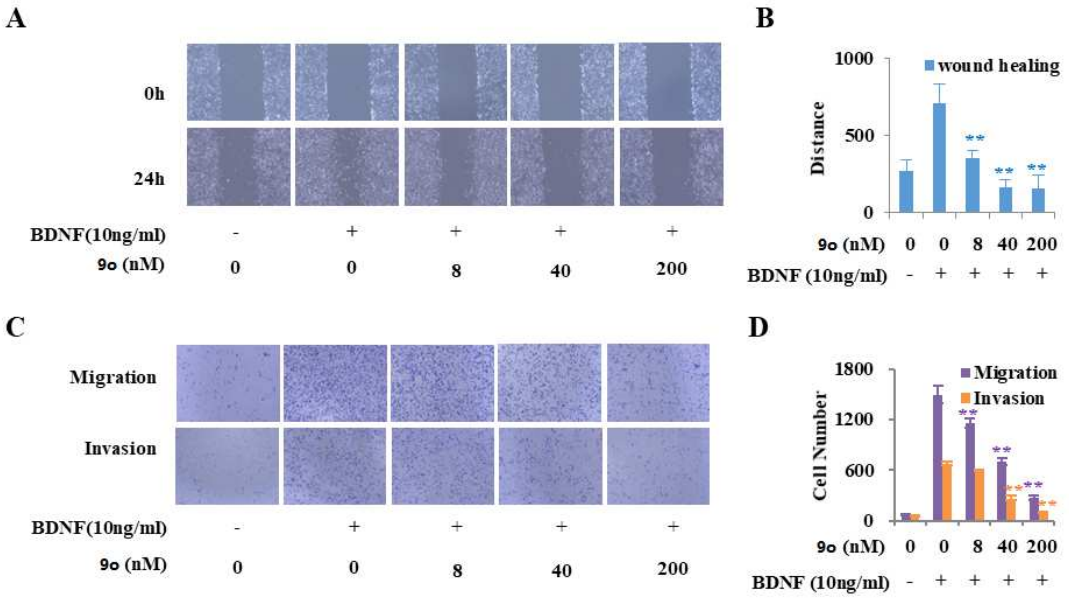

Figure 7. 9o suppresses wound healing, migration and invasion induced by BDNF in SH-SY5Y-TrkB neuroblastoma cells. A) Effect of **9o** on the wound healing induced by BDNF in SH-SY5Y-TrkB neuroblastoma cells. B) Quantitative analysis of wound healing. C) Compound **9o** suppresses migration and invasion induced by BDNF (10 ng/mL) of neuroblastoma cells. D) Quantitative analysis of migration and invasion. The results are presented as the mean ± standard deviation (* $P < 0.05$, ** $P < 0.01$, compare with BDNF treatment by two-tailed Student's *t* test).

The antiproliferative activity of **9o** was also examined against SH-SY5Y-TrkB cell lines. It was shown that **9o** inhibited the proliferation of SH-SY5Y-TrkB cells with an IC_{50} value of 58 nM, which was comparable to that of LOXO-101 (Figure 8). However, both **9o** and LOXO-101exhibited significantly less potency in SH-SY5Y parental cells with low level of TrkB. Further pharmacokinetics investigation also revealed the compound exhibited low blood-brain-barrier (BBB) penetration ability, which may avoid the potential neurotoxicity issue of a pan-Trk inhibitor (Supporting Information).

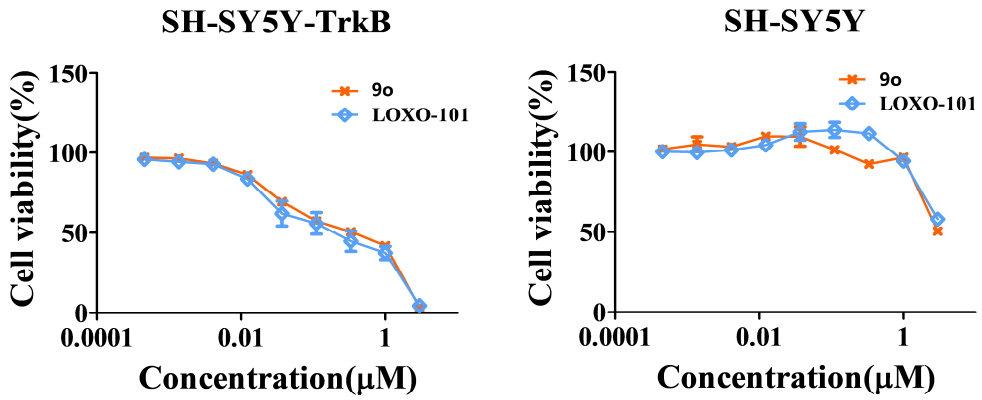

Figure 8. Anti-proliferative activities of compound **9o** and LOXO-101 in SH-SY5Y-TrkB cells. The data were means from at least three independent experiments.

Conclusion

A series of 3-(imidazo[1,2-a]pyrazin-3-ylethynyl)-2-methylbenzamides were designed and synthesized as new selective Trks inhibitors. One of the most promising compounds **9o** exhibited IC_{50} values of 2.65, 10.47, 2.95 nM against TrkA, B and C, respectively. Compound **9o** dose-dependently inhibited the phosphorylation of TrkB and downstream signaling proteins in the SH-SY5Y-TrkB neuroblastoma cells. In addition, **9o** also dose-dependently inhibited the migration and invasiveness of SH-SY5Y-TrkB neuroblastoma cells as well as cellular proliferation. **9o** exhibited the promising anti-proliferative activity against SH-SY5Y-TrkB cells with an IC_{50} of 58 nM. Further pharmacokinetics investigation also suggested that compound **9o** was peripherally restricted, avoiding the potential neurotoxic issue of a pan-Trk inhibitor. Further structural optimization and extensive biological investigation are undergoing and the results will be disclosed in due course.

Experimental section

General Methods for Chemistry

Reagents and solvents were obtained from commercial suppliers and used without further purification. Flash chromatography was performed using silica gel (200-300 mesh or 300-400 mesh). All reactions were monitored by (TLC), and silica gel plates with fluorescence F254 were used and visualized with UV light. ^{1}H and ^{13}C NMR spectra were recorded on a Bruker AV-400 spectrometer at 400 MHz and Bruker AV-500 spectrometer at 125 MHz, respectively. Coupling constants (J) are expressed in hertz (Hz). Chemical shifts (δ) of NMR are reported in parts per million (ppm) units relative to internal control (TMS). The low resolution of ESI-MS was recorded on an Agilent 1200

HPLC-MSD mass spectrometer, and high resolution of ESI-MS was recorded on an Applied Biosystems Q-STAR Elite ESI-LC-MS/MS mass spectrometer. The purity of compounds was determined to be over 95% (>95%) by reverse-phase high performance liquid chromatography (HPLC) analysis. HPLC instrument: DIONEX SUMMIT HPLC (reverse-phase column, Diamonsil C18, 5.0 μm, 4.6 mm × 250 mm (Dikma Technologies); detector, PDA-100 photodiode array; injector, ASI-100 autoinjector; pump: P-680A). Elution: 85% MeOH in water (0.1% ammonia water); flow rate, 1.0 mL/min.

Methyl 3-bromo-5-methylbenzoate (11a). 3-bromo-5-methylbenzoic acid (5.0 g, 23.3 mmol) was dissolved in dry methanol (150 mL) and cooled to 0 °C. Thionyl chloride (5.0 ml, 68.8 mmol) was added dropwise over 10 min. The solution allowed to reach room temperature and then heated to 60 □ for 6 h. Removal of MeOH under reduced pressure resulted in crude product. The crude product was treated with 100 mL water, and a saturated solution of $NaHCO_3$ (50 mL) was added slowly. The aqueous solution was extracted ethyl acetate (3 × 100 mL). The combined organic layers were washed with brine (100 mL), dried over by magnesium sulfate and the solvent was removed in vacuo to get product as yellow oil (5.0 g, 21.8 mmol), yielded 93.6%. ^{1}H NMR (400 MHz, DMSO-d_6) δ 7.84 (s, 1H), 7.76 (s, 1H), 7.71 (s, 1H), 3.85 (s, 3H), 2.37 (s, 3H). LC-MS (ESI) *m/z* 229 $[M + H]^+$.

Methyl 3-ethynyl-5-methylbenzoate (12a). Step (I): To a solution of **11a** (500 mg, 1.81 mmol) and DIPEA (468 mg, 3.62 mmol) in 100 mL dry MeCN, CuI (34 mg, 0.18 mmol) and $Pd(PPh_3)_2Cl_2$ (70 mg, 0.1 mmol) was added. The solution was then degassed with argon for 5 min. Ethynyltrimethylsilane (267 mg, 2.72 mmol) was added dropwise via syringe under argon and the solution was stirred at 80 □ for 12 h. The reaction suspension was cooled to room temperature and filtered through Celite. The solvent was removed by rotary evaporation to get crude mixture. Step (II): The crude mixture was dissolved in 100 mL MeOH, and K_2CO_3 (500 mg, 3.62 mmol) was added to the solution. The suspension was stirred at room temperature for 2 h. The reaction suspension was filtered through Celite, and the solvent was removed by rotary evaporation. The residue was treated with water and extracted with ethyl ether. The combined organic layer was washed with brine and dried by magnesium sulfate. After the removal of solvent via rotary evaporation, the crude product was purified with silica gel column chromatography (ethyl acetate/petroleum ether, v/v = 1/100) to provide methyl 3-ethynyl-5-methylbenzoate (230 mg 1.32 mmol) as light red oil, yield 73%. ^{1}H NMR (400 MHz, DMSO-d_6) δ 7.80 (s, 1H), 7.78 (s, 1H), 7.58 (s, 1H), 4.27 (s, 1H), 3.85 (s, 3H), 2.37 (s, 3H). LC-MS

(ESI) *m/z* 175 $[M + H]^+$.

Methyl 3-(imidazo[1,2-a]pyrazin-3-ylethynyl)-5-methylbenzoate (14a). A round bottom flask was charged with **12a** (250 mg, 0.86 mg), 3-bromoimidazo[1,2-a]pyrazine (255 mg, 1.29 mmol), $Pd(PPh_3)_2Cl_2$ (30 mg, 0.043 mmol), CuI (16 mg, 0.086 mmol). 80 mL dry DMF and DIPEA (333 mg, 2.58 mmol) were added to the flask and the solution was degassed with argon for 5 min. The solution was stirred under argon atmosphere at 80 □ for 18 h. The reaction solution was filtered through Celite and the solvent was removed by rotary evaporation to get crude mixture. The crude mixture was purified with silica gel column chromatography (MeOH/DCM, v/v = 1/100) to provide Mthyl 3-(imidazo[1,2-a]pyrazin-3-ylethynyl)-2-methylbenzoate (160 mg, 0.55 mmol) as light yellow solid, yielded 64%. ^{1}H NMR (400 MHz, DMSO-d_6) δ 9.20 (s, 1H), 8.81 (dd, J^1 = 4.4 Hz, J^2 = 1.2 Hz), 8.23 (s, 1H), 8.12 (d, J = 4.4 Hz), 8.06 (s, 1H), 7.85 (s, 1H), 7.82 (s, 1H). LC-MS (ESI) *m/z* 292 $[M + H]^+$.

3-(imidazo[1,2-a]pyrazin-3-ylethynyl)-5-methyl-*N*-(3-((4-methylpiperazin-1-yl)methyl)-5-(trifluoromethyl)phenyl)benzamide (9a). To a solution of **14a** (160 mg, 0.55 mmol) in anhydrous THF (30 mL), 3-((4-methylpiperazin-1-yl)methyl)-5-(trifluoromethyl)aniline (136 mg, 0.5 mmol) was added. The solution was solution was stirred at -20 □ under argon for 30 minutes, and then t-BuOK solid (185 mg, 1.65 mmol) was added. The temperature allowed to increase to room temperature and the reaction mixture stirred at room temperature for 1 h. The solvent was removed by rotary evaporation. The residue was treated with water and extracted with ethyl ether, then washed with brine, dried over by magnesium sulfate. The organic layer was concentrated under reduced pressure. The residue was purified by silica gel column chromatography (MeOH/DCM, v/v = 1/40) to afford the target compound (130 mg, 0.24 mmol), light yellow solid, yielded 44.4%. ^{1}H NMR (400 MHz, DMSO-d_6) δ 10.62 (s, 1H), 9.21 (s, 1H), 8.79 (d, J = 4.4 Hz, 1H), 8.25 (s, 1H), 8.19 (s, 1H), 8.14 (d, J = 4.8 Hz, 1H), 8.12 (s, 1H), 8.03 (s, 1H), 7.88 (s, 1H), 7.80 (s, 1H), 7.37 (s, 1H), 3.56 (s, 2H), 2.46 (s, 3H), 2.42 (br, 8H), 2.21 (s, 3H). ^{13}C NMR (125 MHz, DMSO-d_6) δ 164.9, 143.2, 140.7, 140.3, 139.8, 139.4, 138.8, 135.0, 134.6, 130.7, 129.2, 129.2 (q, J = 31.5 Hz), 127.5, 124.1 (q, J = 270.5 Hz), 123.8, 121.4, 120.1, 119.1, 115.1, 108.9, 99.3, 75.8, 61.3, 54.5, 52.2, 45.4, 20.7. HRMS (ESI) calcd for $C_{29}H_{27}F_3N_6O$ $[M + H]^+$ 533.2271, found 533.2258. Purity 96.6% (t_R = 13.83 min).

5-(imidazo[1,2-a]pyrazin-3-ylethynyl)-2-methyl-*N*-(3-((4-methylpiperazin-1-yl)methyl)-5-(trifluoromethyl)phenyl)benzamide (9b). Compound **9b** was prepared by following a similar procedure to that for **9a**. ^{1}H NMR (400 MHz, DMSO-d_6) δ 10.75 (s, 1H), 9.20 (s, 1H), 8.79 (d, J = 4.0

Hz, 1H), 8.22 (s, 1H), 8.16 (s, 1H), 8.11 (d, *J* = 4.4 Hz), 7.93 (d, *J* = 3.2 Hz, 2H), 7.74 (d, *J* = 7.6 Hz, 1H), 7.45 (d, *J* = 8.0 Hz, 1H), 7.37 (s, 1H), 3.55 (s, 1H), 2.45 (s, 3H), 2.40 (br, 8H), 2.18 (s, 3H). ^{13}C NMR (125 MHz, DMSO-d_6) δ 167.0, 143.1, 140.8, 140.2, 139.8, 139.2, 137.2, 136.9, 132.2, 131.2, 130.6, 130.2, 129.3 (q, *J* = 31.0 Hz), 124.1 (q, *J* = 270.6 Hz), 123.2, 119.9, 119.1, 118.7, 114.5, 109.0, 99.3, 75.6, 61.2, 54.5, 52.3, 45.5, 19.4. HRMS (ESI) calcd for $C_{29}H_{27}F_3N_6O$ [M + H] $^+$ 533.2271, found 533.2253. Purity 98.1% (t_R = 10.96 min).

3-(imidazo[1,2-a]pyrazin-3-ylethynyl)-2-methyl-*N*-(3-((4-methylpiperazin-1-yl)methyl)-5-(trifluoromethyl)phenyl)benzamide (9c). Compound **9c** was prepared by following a similar procedure to that for **9a**. ^{1}H NMR (400 MHz, DMSO-d_6) δ 10.76 (s, 1H), 9.21 (s, 1H), 8.67 (d, *J* = 4.4 Hz, 1H), 8.27 (s, 1H), 8.15 (s, 1H), 8.13 (d, *J* = 4.4 Hz, 1H), 7.92 (s, 1H), 7.84 (d, *J* = 8.0 Hz, 1H), 7.59 (d, *J* = 7.6 Hz, 1H), 7.44 (t, *J* = 7.7 Hz, 1H), 7.37 (s, 1H), 3.54 (s, 2H), 2.61 (s, 3H), 2.40 (br, 8H), 2.16 (s, 3H). ^{13}C NMR (125 MHz, DMSO-d_6) δ 167.5, 143.2, 141.0, 140.3, 139.8, 139.5, 137.7, 136.7, 133.1, 130.8, 129.3 (q, *J* = 31.2 Hz), 128.2, 126.1, 124.1 (q, *J* = 270.7 Hz), 123.1, 122.5, 120.0, 119.0, 114.4, 109.0, 98.2, 79.8, 61.2, 54.6, 52.4, 45.6, 17.9. HRMS (ESI) calcd for $C_{29}H_{27}F_3N_6O$ [M + H] $^+$ 533.2271, found 533.2257. Purity 99.3% (t_R = 11.45 min).

3-(imidazo[1,2-a]pyrazin-3-ylethynyl)-*N*-(3-((4-methylpiperazin-1-yl)methyl)-5-(trifluoromethyl)phenyl)benzamide (9d). Compound **9d** was prepared by following a similar procedure to that for **9a**. ^{1}H NMR (400 MHz, DMSO-d_6) δ 10.69 (s, 1H), 9.22 (d, *J* = 1.3 Hz, 1H), 8.82 (dd, J^1 = 4.5 Hz, J^2 = 1.3 Hz, 1H), 8.35 (s, 1H), 8.26 (s, 1H), 8.20 (s, 1H), 8.14 (d, *J* = 4.4 Hz, 1H), 8.05 (d, *J* = 8.0 Hz, 2H), 7.95 (d, *J* = 7.7 Hz, 1H), 7.67 (t, *J* = 7.8 Hz, 1H), 7.38 (s, 1H), 3.57 (s, 2H), 2.43 (br, 8H), 2.22 (s, 3H). ^{13}C NMR (125 MHz, DMSO-d_6) δ 164.9, 143.2, 140.6, 140.3, 139.8, 139.5, 134.9, 134.2, 130.7, 130.3, 129.2 (q, *J* = 31.3 Hz), 129.1, 128.7, 124.1 (q, *J* = 270.7 Hz), 123.9, 121.5, 120.1, 119.2, 115.2, 115.1, 108.8, 99.1, 76.2, 61.3, 54.4, 52.1, 45.4. HRMS (ESI) calcd for $C_{28}H_{25}F_3N_6O$ [M + H] $^+$ 519.2115, found 519.2100. Purity 99.5% (t_R = 11.82 min).

2-chloro-3-(imidazo[1,2-a]pyrazin-3-ylethynyl)-*N*-(3-((4-methylpiperazin-1-yl)methyl)-5-(trifluoromethyl)phenyl)benzamide (9e). Compound **9e** was prepared by following a similar procedure to that for **9a**. ^{1}H NMR (400 MHz, DMSO-d_6) δ 10.95 (s, 1H), 9.24 (d, *J* = 1.2 Hz, 1H), 8.67 (dd, J^1 = 4.4 Hz, J^2 = 1.2 Hz), 8.31 (s, 1H), 8.17 (d, *J* = 4.8 Hz, 1H), 8.12 (s, 1H), 7.99 (dd, J^1 = 8.0 Hz, J^2 = 1.6 Hz, 1H), 7.88 (s, 1H), 7.72 (dd, J^1 = 7.6 Hz, J^2 = 1.2 Hz, 1H), 7.59 (t, *J* = 7.6 Hz, 1H), 7.39 (s, 1H), 3.55 (s, 2H), 2.40 (br, 4H), 2.33 (br, 4H), 2.15 (s, 3H). ^{13}C NMR (125 MHz, DMSO-d_6) δ

164.7, 143.3, 141.2, 140.5, 139.9, 139.5, 137.5, 134.0, 131.1, 130.7, 129.4 (d, J = 30.5 Hz), 129.3, 127.6, 124.1 (q, J = 269.9 Hz), 123.0, 122.2, 120.2, 118.9, 114.3, 108.5, 96.2, 81.1, 61.2, 54.7, 52.5, 45.7, 29.0. HRMS (ESI) calcd for $C_{28}H_{24}ClF_3N_6O$ $[M + H]^+$ 553.1725, found 553.1726. Purity 97.8% (t_R = 11.64 min).

3-(imidazo[1,2-a]pyrazin-3-ylethynyl)-2-methoxy-*N*-(3-((4-methylpiperazin-1-yl)methyl)-5-(trifluoromethyl)phenyl)benzamide (9f). Compound **9f** was prepared by following a similar procedure to that for **9a**. ^{1}H NMR (400 MHz, DMSO-d_6) δ 10.75 (s, 1H), 9.22 (d, J = 1.2 Hz, 1H), 8.64 (dd, J^1 = 4.4 Hz, J^2 = 1.2 Hz, 1H), 8.27 (s, 1H), 8.16 (d, J = 4.4 Hz, 2H), 7.91 (s, 1H), 7.87 (dd, J^1 = 7.6 Hz, J^2 = 1.6 Hz, 1H), 7.66 (dd, J^1 = 7.6 Hz, J^2 = 1.4 Hz, 1H), 7.38 (s, 1H), 7.34 (t, J = 7.6 Hz, 1H), 4.03 (s, 3H), 3.54 (s, 2H), 2.39 (br, 4H), 2.33 (br, 4H), 2.15 (s, 3H). ^{13}C NMR (125 MHz, DMSO-d_6) δ 164.9, 157.6, 143.3, 141.0, 140.3, 139.7, 139.5, 135.0, 131.1, 130.9, 130.2, 129.4 (d, J = 31.1 Hz), 124.1 (q, J = 270.8 Hz), 124.1, 123.1, 120.0, 118.8, 115.9, 114.4, 108.9, 95.8, 80.0, 62.3, 61.2, 54.7, 52.5, 45.7. HRMS (ESI) calcd for $C_{29}H_{27}F_3N_6O_2$ $[M + H]^+$ 533.1725, found 533.1726. Purity 95.8% (t_R = 11.30 min).

2-ethyl-3-(imidazo[1,2-a]pyrazin-3-ylethynyl)-*N*-(3-((4-methylpiperazin-1-yl)methyl)-5-(trifluoromethyl)phenyl)benzamide (9g). Compound **9g** was prepared by following a similar procedure to that for **9a**. ^{1}H NMR (400 MHz, DMSO-d_6) δ 10.80 (s, 1H), 9.21 (s, 1H), 8.62 (dd, J^1 = 4.6 Hz, J^2 = 1.4 Hz, 1H), 8.26 (s, 1H), 8.15 (d, J = 4.4 Hz, 2H), 7.91 (s, 1H), 7.85 (dd, J^1 = 7.6 Hz, J^2 = 0.8 Hz, 1H), 7.59 (d, J = 6.8 Hz, 1H), 7.45 (t, J = 7.8 Hz, 1H), 7.37 (s, 1H), 3.54 (s, 2H), 3.01 (q, J = 7.3 Hz, 2H), 2.39 (br, 4H), 2.15 (br, 4H), 1.99 (s, 3H), 1.30 (t, J = 7.4 Hz, 3H). ^{13}C NMR (125 MHz, DMSO-d_6) δ 167.5, 143.1, 143.0, 140.9, 140.2, 139.7, 139.4, 137.2, 133.5, 130.7, 129.2 (q, J = 31.2 Hz), 128.2, 126.1, 124.0 (q, J = 270.6 Hz), 123.0, 121.7, 119.8, 118.7, 114.3, 108.9, 97.8, 78.9, 61.2, 54.6, 52.4, 45.6, 24.9, 15.3. HRMS (ESI) calcd for $C_{30}H_{29}F_3N_6O$ $[M + H]^+$ 547.2428, found 547.2418. Purity 99.8% (t_R = 11.82 min).

3-(imidazo[1,2-a]pyrazin-3-ylethynyl)-*N*-(3-((4-methylpiperazin-1-yl)methyl)-5-(trifluoromethyl)phenyl)-2-propylbenzamide (9h). Compound **9h** was prepared by following a similar procedure to that for **9a**. ^{1}H NMR (400 MHz, DMSO-d_6) δ 10.80 (s, 1H), 9.21 (s, 1H), 8.62 (d, J = 4.4 Hz, 1H), 8.25 (s, 1H), 8.15 (d, J = 4.4 Hz, 1H), 8.12 (s, 1H), 7.91 (s, 1H), 7.85 (d, J = 7.7 Hz, 1H), 7.59 (d, J = 7.2 Hz, 1H), 7.45 (t, J = 7.5 Hz, 1H), 7.37 (s, 1H), 3.54 (s, 2H), 3.00 (t, J = 6.8 Hz, 2H), 2.39 (br, 4H), 2.33 (br, 4H), 2.15 (s, 3H), 1.71 (q, J = 6.8 Hz, 2H), 0.94 (t, J = 7.0 Hz, 3H). ^{13}C NMR

(125 MHz, DMSO-d_6) δ 167.7, 143.3, 141.6, 141.1, 140.3, 139.9, 139.6, 137.5, 133.6, 130.8, 129.4 (d, J = 31.2 Hz), 128.4, 126.3, 124.2 (q, J = 268.6 Hz), 123.3, 122.2, 120.1, 118.8, 114.5, 109.1, 98.3, 79.0, 61.3, 54.7, 52.5, 45.7, 33.4, 23.9, 14.2. HRMS (ESI) calcd for $C_{31}H_{31}F_3N_6O$ $[M + H]^+$ 561.2584, found 561.2577. Purity 96.5% (t_R = 11.60 min).

3-(imidazo[1,2-a]pyrazin-3-ylethynyl)-2-isopropyl-*N*-(3-((4-methylpiperazin-1-yl)methyl)-5-(trifluoromethyl)phenyl)benzamide (9i). Compound **9i** was prepared by following a similar procedure to that for **9a**. ^{1}H NMR (400 MHz, DMSO-d_6) δ 10.85 (s, 1H), 9.21 (s, 1H), 8.62 (d, J = 4.4 Hz, 1H), 8.25 (s, 1H). 8.15 (d, J = 4.8 Hz, 2H), 7.90 (s, 1H), 7.85 (d, J = 7.6 Hz, 1H), 7.51 (d, J =7.6 Hz, 1H), 7.42 (t, J = 7.6 Hz, 1H), 7.37 (s, 1H), 3.54 (s, 2H), 3.50-3.45 (m, 1H), 2.39 (br, 4H), 2.33 (br, 4H), 2.15 (s, 3H), 1.50 (d, J = 7.0 Hz, 6H). ^{13}C NMR (125 MHz, DMSO-d_6) δ 168.4, 145.5, 143.3, 141.1, 140.3, 139.8, 139.4, 138.0, 134.9, 130.9, 129.4 (d, J = 31.1 Hz), 128.3, 126.2, 124.1 (q, J = 269.3Hz), 123.1, 120.6, 120.0, 118.9, 114.3, 109.1, 99.1, 80.4, 61.2, 54.7, 52.5, 45.7, 32.0, 21.4. HRMS (ESI) calcd for $C_{31}H_{31}F_3N_6O$ $[M + H]^+$ 561.2584, found 561.2584. Purity 95.5% (t_R = 11.60 min).

3-((6-(4-((tert-butoxycarbonyl)amino)phenyl)imidazo[1,2-a]pyrazin-3-yl)ethynyl)-2-methylbenzoic acid (15). A solution of methyl 3-((6-(4-((tert-butoxycarbonyl)amino) phenyl)imidazo[1,2-a]pyrazin-3-yl)ethynyl)-2-methylbenzoate (prepared by following a similar procedure to that for **14a**; 1.5 g, 3.11 mmol) in 200 ml of THF/H_2O (2:1) was treated with LiOH (372 mg, 15.5 mmol) in 10 ml water. The mixture was stirred at 25 °C for 4 h. The solvent was removed under reduced pressure and the resulting solution was diluted with 100 ml water, then acidified with 1 M HCl to pH = 5-7. The resulting solid was filtered to afford of 3-((6-(4-((tert-butoxycarbonyl)amino)phenyl)imidazo[1,2-a] pyrazin-3-yl)ethynyl)-2-methylbenzoic acid (1.1 g, 2.35 mmol) as white solid, yielded 75.5%. ^{1}H NMR (400 MHz, DMSO-d_6) δ 9.55 (s, 1H), 9.24 (d, J = 1.2 Hz, 1H), 8.86 (d, J = 1.6 Hz, 1H), 8.22 (s, 1H), 8.03 (d, J = 8.4 Hz, 2H), 7.81 (d, J = 7.2 Hz, 1H), 7.61 (d, J = 8.8 Hz, 2H), 7.33 (s, J = 8.0 Hz, 1H), 2.76 (s, 3H), 1.49 (s, 9H). LC-MS (ESI) *m/z* 467 $[M - H]^-$.

3-((6-(4-aminophenyl)imidazo[1,2-a]pyrazin-3-yl)ethynyl)-2-methyl-*N*-(3-((4-methylpiperazin-1-yl)methyl)-5-(trifluoromethyl)phenyl)benzamide (9j). Step (I): To a solution of **15** (250 mg, 0.53 mmol) and 3-((4-methylpiperazin-1-yl)methyl)-5-(trifluoromethyl)aniline (136 mg, 0.5 mmol) in anhydrous DMF (10 mL), was added HATU (380 mg, 1.0 mmol) and 0.3 ml DIPEA (235 mg, 1.82 mmol). The solution was stirred for 6 h at room temperature. The solution was diluted with 20 ml water,

then the resulting solid was filtered to afford crude mixture. The crude mixture was purified with silica gel column chromatography (MeOH/DCM, v/v = 1/30) to provide tert-butyl(4-(3-((2-methyl-3-((3-((4-methylpiperazin-1-yl)methyl)-5-(trifluoromethyl)phenyl)carbamoyl)phenyl)ethynyl)imidazo[1,2-a]pyrazin-6-yl)phenyl)carbamate (207 mg, 0.28 mmol) as yellow solid, yield 56.0%. LC-MS (ESI) *m/z* 724 $[M + H]^+$. Step (II): The product of last step (207 mg, 0.28 mmol) was dissolved in 50mL of CF_3COOH/DCM (1:1). The solution was stirred for 6 h at room temperature. The solvent was removed by rotary evaporation, and then diluted with 10 mL MeOH. The MeOH solution was alkalified with 1 M KOH to pH = 9-11. The solution was treated with water and extracted with ethyl ether, then washed with brine, dried over by anhydrous sodium sulfate. The organic layer was concentrated under reduced pressure. The residue was purified by silica gel column chromatography (MeOH/DCM, v/v = 1:30) to afford the target compound (129 mg, 0.21 mmol), white solid, yielded 75.0%. ^{1}H NMR (400 MHz, DMSO-d_6) δ 10.79 (s, 1H), 9.20 (s, 1H), 8.71 (s, 1H), 8.21 (d, J = 2.8 Hz, 1H), 8.13 (s, 1H), 7.97 (s, 1H), 7.90 (d, J = 3.6 Hz, 1H), 7.81 (d, J = 5.7 Hz, 2H), 7.59 (s, 1H), 7.45 (s, 1H), 7.40 (s, 1H), 6.68 (d, J = 5.7 Hz, 2H), 5.45 (s, 2H), 3.60 (s, 2H), 2.74 (br, 4H), 2.64 (s, 3H). ^{13}C NMR (125 MHz, DMSO-d_6) δ 167.6, 158.1, 157.9, 149.8, 142.1, 140.8, 139.9, 139.8, 139.3, 137.6, 136.8, 133.2, 129.5 (d, J = 31.8 Hz), 128.1, 127.2, 126.1, 124.1 (q, J = 272.9 Hz), 123.3, 122.8, 120.1, 118.4, 116.0, 114.7, 113.9, 111.7, 109.2, 98.5, 80.2, 60.8, 53.7, 50.9, 44.0, 17.9. HRMS (ESI) calcd for $C_{35}H_{32}F_3N_7O$ $[M + H]^+$ 624.2693, found 624.2666. Purity 97.0% (t_R = 13.31 min).

2-methyl-*N*-(3-((4-methylpiperazin-1-yl)methyl)-5-(trifluoromethyl)phenyl)-3-((6-phenylimidazo[1,2-a]pyrazin-3-yl)ethynyl)benzamide (9k). Compound **9k** was prepared by following a similar procedure to that for **9a**. ^{1}H NMR (400 MHz, DMSO-d_6) δ 10.78 (s, 1H), 9.31 (d, J = 0.8 Hz, 1H), 8.98 (s, 1H), 8.29 (s, 1H), 8.17 (s, 1H), 8.14 (d, J = 7.5 Hz, 2H), 7.90 (d, J = 8.0 Hz, 2H), 7.61 (d, J = 7.6 Hz, 1H), 7.54 (t, J = 7.4 Hz, 2H), 7.45 (t, J = 7.4 Hz, 2H), 7.37 (s, 1H), 3.54 (s, 2H), 2.65 (s, 3H), 2.40 (br, 4H), 2.33 (br, 4H), 2.15 (s, 3H). ^{13}C NMR (125 MHz, DMSO-d_6) δ 167.6, 142.5, 140.9, 140.1, 140.0, 139.6 (d, J = 4.8 Hz), 137.7, 136.9, 135.8, 133.2, 129.3 (q, J = 31.1 Hz), 128.8, 128.2, 126.3, 126.0, 124.1 (q, J = 270.8 Hz), 123.2, 122.6, 119.9, 114.8, 114.4, 109.8, 98.6, 79.9, 61.3, 54.7, 52.5, 45.7, 17.9. HRMS (ESI) calcd for $C_{35}H_{31}F_3N_6O$ $[M + H]^+$ 609.2584, found 609.2580. Purity 98.4% (t_R = 20.22 min).

2-methyl-*N*-(3-((4-methylpiperazin-1-yl)methyl)-5-(trifluoromethyl)phenyl)-3-((6-(pyridin-4-yl)imidazo[1,2-a]pyrazin-3-yl)ethynyl)benzamide (9l). Compound **9l** was prepared by following a

similar procedure to that for **9a**. ^{1}H NMR (400 MHz, DMSO-d_6) δ 10.80 (s, 1H), 9.35 (d, J = 1.2 Hz, 1H), 9.22 (s, 1H), 8.73 (d, J = 5.6 Hz, 2H), 8.34 (s, 1H), 8.18 (s, 1H), 8.15 (d, J = 6.0 Hz, 2H), 7.93 (d, J = 7.4 Hz, 1H), 7.92 (s, 1H), 7.62 (d, J = 7.5 Hz, 1H), 7.47 (t, J = 7.7 Hz, 1H), 7.37 (s, 1H), 3.54 (s, 2H), 2.66 (s, 3H), 2.39 (br, 4H), 2.33 (br, 4H), 2.15 (s, 3H). ^{13}C NMR (125 MHz, DMSO-d_6) δ 167.6, 150.4, 143.1, 142.9, 141.0, 140.6, 139.9, 137.7, 137.1, 136.8, 133.4, 129.4 (q, J = 30.9 Hz), 128.3, 126.1, 124.2 (q, J = 260.0 Hz), 122.6, 120.5, 117.0, 114.4, 110.3, 98.7, 79.7, 61.3, 54.7, 52.5, 45.8, 29.0, 17.9. HRMS (ESI) calcd for $C_{34}H_{30}F_3N_7O$ [M + H] $^{+}$ 610.2537, found 610.2512. Purity 98.1% (t_R = 13.88 min).

3-((6-(4-aminophenyl)imidazo[1,2-a]pyrazin-3-yl)ethynyl)-2-methyl-*N*-(3-methyl-5-((4-methylpiperazin-1-yl)methyl)phenyl)benzamide (9m). Compound **9m** was prepared by following a similar procedure to that for **9j**. ^{1}H NMR (400 MHz, DMSO-d_6) δ 10.35 (s, 1H), 9.20 (s, 1H), 8.70 (s, 1H), 8.20 (s, 1H), 7.86 (d, J = 7.6 Hz, 1H), 7.81 (d, J = 8.3 Hz, 2H), 7.53 (d, J = 8.8 Hz, 1H), 7.50 (d, J = 9.4 Hz, 1H), 7.42 (t, J = 7.5 Hz, 1H), 6.85 (s, 1H), 6.68 (d, J = 8.3 Hz, 2H), 5.44 (s, 2H), 3.39 (s, 2H), 2.63 (s, 3H), 2.44-2.21 (br, 8H), 2.29 (s, 3H), 2.14 (s, 3H). ^{13}C NMR (125 MHz, DMSO-d_6) δ 167.1, 149.8, 142.1, 140.8, 139.7, 139.3, 138.9, 138.8, 138.3, 137.6, 136.6, 132.8, 128.0, 127.9, 127.2, 126.0, 124.9, 122.8, 122.6, 118.8, 117.3, 113.9, 111.7, 109.2, 98.6, 80.0, 79.1, 62.2, 54.7, 52.6, 45.7, 21.2, 17.9. HRMS (ESI) calcd for $C_{35}H_{35}N_7O$ [M + H] $^{+}$ 570.2976, found 570.2957. Purity 99.8% (t_R = 8.91 min).

3-((6-(4-aminophenyl)imidazo[1,2-a]pyrazin-3-yl)ethynyl)-*N*-(3-ethyl-5-((4-methylpiperazin-1-yl)methyl)phenyl)-2-methylbenzamide (9n). Compound **9n** was prepared by following a similar procedure to that for **9j**. ^{1}H NMR (400 MHz, DMSO-d_6) δ 10.35 (s, 1H), 9.19 (s, 1H), 8.70 (s, 1H), 8.20 (s, 1H), 7.86 (d, J = 7.6 Hz, 1H), 7.81 (d, J = 7.6 Hz, 2H), 7.53 (d, J = 5.8 Hz, 3H), 7.42 (t, J = 7.2 Hz, 1H), 6.88 (s, 1H), 6.68 (d, J = 7.9 Hz, 2H), 5.43 (s, 2H), 3.41 (s, 2H), 2.63 (s, 2H), 2.59 (q, J = 7.6 Hz, 2H), 2.37 (br, 4H), 2.33 (br, 4H), 2.15 (s, 3H). ^{13}C NMR (125 MHz, DMSO-d_6) δ 167.1, 149.8, 144.0, 142.1, 140.8, 139.7, 139.3, 139.0, 138.9, 138.3, 136.6, 132.8, 128.0, 127.2, 126.0, 123.7, 122.8, 122.6, 117.7, 117.5, 113.9, 111.7, 109.2, 98.6, 80.0, 62.2, 54.7, 52.6, 45.7, 28.2, 17.9, 15.5. HRMS (ESI) calcd for $C_{36}H_{37}N_7O$ [M + H] $^{+}$ 584.3132, found 584.3115. Purity 99.6% (t_R = 10.23 min).

3-((6-(4-aminophenyl)imidazo[1,2-a]pyrazin-3-yl)ethynyl)-*N*-(3-isopropyl-5-((4-methylpiperazin-1-yl)methyl)phenyl)-2-methylbenzamide (9o). Compound **9o** was prepared by following a similar procedure to that for **9j**. ^{1}H NMR (400 MHz, DMSO-d_6) δ 10.34 (s, 1H), 9.19 (d, J = 1.6 Hz, 1H), 8.70

(d, *J* = 1.2 Hz, 1H), 8.20 (s, 1H), 7.86 (d, *J* = 7.6 Hz, 1H), 7.81 (d, *J* = 8.8 Hz, 2H), 7.56 (d, *J* = 4.0 Hz, 2H), 7.53 (s, 1H), 7.42 (t, *J* = 8.0 Hz, 1H), 6.91 (s, 1H), 6.68 (d, *J* = 8.4 Hz, 2H), 5.42 (s, 2H), 3.42 (s, 2H), 2.90-2.83 (m, 1H), 2.64 (s, 3H), 2.37-2.33 (br, 8H), 2.15 (s, 3H), 1.21 (d, *J* = 7.6 Hz, 2H). ^{13}C NMR (125 MHz, DMSO-d_6) δ 167.1, 149.7, 148.7, 142.1, 140.8, 139.7, 139.3, 139.0, 138.8, 138.3, 136.6, 132.8, 128.0, 127.2, 125.9, 122.8, 122.6, 122.3, 117.6, 116.2, 113.9, 111.7, 109.2, 98.6, 80.0, 62.3, 54.7, 52.6, 45.7, 33.4, 23.9, 17.9. HRMS (ESI) calcd for $C_{37}H_{39}N_7O$ [M + H] $^+$ 598.3289, found 598.3276. Purity 95.1% (t_R = 12.93 min).

3-((6-(4-aminophenyl)imidazo[1,2-a]pyrazin-3-yl)ethynyl)-*N*-(3-(tert-butyl)-5-((4-methylpiperazin-1-yl)methyl)phenyl)-2-methylbenzamide (9p). Compound **9p** was prepared by following a similar procedure to that for **9j**. ^{1}H NMR (400 MHz, DMSO-d_6) δ 10.35 (s, 1H), 9.19 (d, *J* = 1.2 Hz, 1H), 8.70 (d, *J* = 1.2 Hz, 1H), 8.20 (s, 1H), 7.86 (d, *J* = 6.8 Hz, 1H), 7.81 (d, *J* = 8.4 Hz, 2H), 7.66 (s, 1H), 7.63 (s, 1H), 7.54 (d, *J* = 7.2 Hz, 2H), 7.42 (t, *J* = 7.6 Hz, 1H), 6.69 (s, 1H), 6.68 (d, *J* = 8.4 Hz, 2H), 5.44 (s, 2H), 3.45 (s, 2H), 2.64 (s, 3H), 2.40 (br, 8H), 2.19 (s, 3H), 2.03-1.95 (m, 1H), 1.28 (s, 9H). ^{13}C NMR (125 MHz, DMSO-d_6) δ 167.1, 151.0, 149.7, 142.1, 140.8, 139.7, 138.8, 138.3, 136.6, 132.8, 129.6, 128.0, 127.2, 125.9, 122.8, 122.6, 121.1, 117.2, 115.3, 113.9, 111.7, 98.6, 80.0, 62.3, 54.6, 52.3, 45.5, 34.4, 31.1, 17.9. HRMS (ESI) calcd for $C_{38}H_{41}N_7O$ [M + H] $^+$ 612.3445, found 612.3435. Purity 98.0% (t_R = 13.13 min).

3-((6-(4-aminophenyl)imidazo[1,2-a]pyrazin-3-yl)ethynyl)-2-methyl-*N*-(5-((4-methylpiperazin-1-yl)methyl)-[1,1'-biphenyl]-3-yl)benzamide (9q). Compound **9q** was prepared by following a similar procedure to that for **9j**. ^{1}H NMR (400 MHz, DMSO-d_6) δ 10.53 (s, 1H), 9.20 (s, 1H), 8.71 (s, 1H), 8.32 (s, 1H), 8.21 (s, 1H), 8.00 (s, 1H), 7.88 (d, *J* = 7.5 Hz, 1H), 7.82 (d, *J* = 8.4 Hz, 2H), 7.72 (s, 1H), 7.62 (d, *J* = 7.6 Hz, 2H), 7.59 (d, *J* = 7.6 Hz, 1H), 7.51-7.37 (m, 4H), 7.31 (s, 1H), 6.68 (d, *J* = 8.5 Hz, 2H), 5.44 (s, 2H), 3.52 (s, 2H), 2.66 (s, 3H), 2.42 (br, 4H), 2.34 (br, 4H), 2.15 (s, 3H). ^{13}C NMR (125 MHz, DMSO-d_6) δ 167.3, 149.7, 142.1, 140.8, 140.6, 140.2, 139.7, 139.6, 139.3, 138.2, 136.7, 132.9, 129.0, 128.0, 127.5, 127.2, 126.6, 126.0, 122.8, 122.7, 122.5, 119.0, 116.7, 113.9, 111.7, 109.2, 98.6, 80.0, 79.1, 62.1, 54.7, 52.6, 45.7, 17.9. HRMS (ESI) calcd for $C_{40}H_{37}N_7O$ [M + H] $^+$ 632.3132, found 632.3111. Purity 97.0% (t_R = 11.73 min).

Computational Study

The crystal structures of TrkC and Abl were taken from PDB ID 3V5Q and 3OXZ. Hydrogen atoms and charges were added during a brief relaxation performed using the "Protein Preparation

Wizard" workflow in Maestro 11.7 (Schrodinger LLC). All HETATM residues and crystal water molecules were removed. After the hydrogen bond network was optimized, the crystal structures were minimized until the RMSD between the minimized structure and the starting structure reached 0.3 Å with OPLS 2005 force field. The grid-enclosing box was placed on the centroid of the binding ligand in the optimized crystal structure as described above, and accept the remaining default values. The structure of compound **8** was optimized with Lig-prep module in Maestro to afford multi conformations. Standard precision (SP) approach of Glide was adopted with the default parameters, and the top-ranking pose was retained as the reasonable binding pose.

Crystallization and Structure Determination.

The kinase domain of human TrkC (residues 526-839) was expressed as an N-terminal hexahistidine-SUMO fusion in *E. Coli* cells and purified by Nickel affinity chromatography. The tag was cleaved with ULP1 protease. The proteins were further fractioned by ion exchange chromatography on a Q column (GE Healthcare) and size exclusion chromatography on a Superdex-75 column (GE Healthcare). To form complex, TrkC in 25mM Tris pH 8.0, 100 mM NaCl, 5 mM DTT was incubated with 1 mM compound **9c** and **9o**, respectively. Hanging drops were set up with diffracting crystals obtained from a 1:1 ratio of protein to mother liquor (0.1 M MES, pH 6.0, 0.15 M $(NH_4)_2SO_4$, 15% PEG 4000). Prior to flash frozen in liquid nitrogen, crystals were equilibrated in mother liquor supplemented with 25%~30% glycerol. All data sets were collected on beam-line BL17U1 at Shanghai Synchrotron Radiation Facility. Data were indexed, integrated and scaled using HKL2000 package [46]. Initial phases were identified using molecular replacement in Phaser [47]. Iterative cycles of model building and refinement were carried out using COOT [48] and PHENIX [49].

In vitro enzymatic activity assay

The kinases and Z'-Lyte Kinase Assay Kit were commercially purchased from Invitrogen.

Firstly, TrkA/B/C and the Z'-Lyte Kinase Assay Kit were purchased from Invitrogen. The assays were performed according to the manufacturer's instructions. The concentrations of kinases were determined by optimization experiments and the concentrations used were 1.22 ng/μL, 0.056 ng/μL and 1.73 ng/μL. First, the solutions of the compounds were diluted from $1x10^{-10}$M to $1x10^{-4}$M in DMSO and a 400 μM compound solution was prepared (4 μL compound dissolved in 96 μL water). Second, a 100 μM ATP solution in 1.33 X kinase buffer was prepared. Third, a kinase/peptide mixture containing 2 X kinase

and 4 μM Tyr1 peptide (PV3190; Invitrogen, Waltham, MA, USA) was prepared immediately before use. A kinase/peptide mixture was prepared by diluting Z'-Lyte Tyr1 peptide (PV3190; Invitrogen) and kinase in 1 X Kinase Buffer, and an 0.2 μM Tyr1 phospho-peptide solution was made by adding Z'-Lyte Tyr1 phosphopeptide to 1 X Kinase Buffer. The final 10 μL reaction solution consists of 12.2 ng TrkA/0.56 ng TrkB/17.3 ng TrkC, 2 μM Tyr1 peptide in 1 X kinase buffer. For each assay, 10 μL kinase reactions, including 2.5 μL compound solution, 5 μL Kinase/Peptide Mixture, and 2.5 μL ATP solution were made at first. The plate wells were mixed thoroughly and incubated for 1 h at room temperature. Then 5 μL development solution was added to each well and the plate was incubated for 1 h at room temperature; the phosphopeptides were cleaved at this time. Finally, 5 μL of stop reagent was added to stop the reaction. For the control setting, 5 μL phospho-peptide solution instead of the kinase/peptide mixture was used as a 100% phosphorylation control. 2.5 μL 1.33 X kinase buffer instead of ATP solution was used as a 100% inhibition control, and 2.5 μL 4% DMSO instead of compound solution was used as the 0% inhibitor control. The plate was measured on an EnVision Multilabel Reader (Perkin-Elmer). Curve fitting and data presentation was performed using GraphPad Prism, version 5.0. Every experiment was repeated at least three times.

Secondly, the kinase Abl1 was P3049, and it was full-length human recombinant protein expressed in insect cells and histidine-tagged. Inhibition activities of inhibitors against Abl1 were performed in 384-well plates using the FRET-based Z′-Lyte assay system according to the manufacturer's instructions (Invitrogen). Briefly, the kinase substrate was diluted into 5 μL of 1X kinase reaction buffer; and the kinase was added. Compounds (10 nL) with indicated concentrations were then delivered to the reaction by using Echo liquid handler, and the mixture was incubated for 30 min at room temperature. Then 5 μL of 2X ATP solution was added to initiate the reaction, and the mixture was further incubated for 2 h at room temperature. The resulting reactions contained 10 μM of ATP, 2 μM of Tyr2 Peptide substrate in 50 mM HEPES (PH 7.5), 0.01% BRIJ-35, 10 mM $MgCl_2$, 1 mM EGTA, 0.0247 μg/mL Abl1, and inhibitors as appropriate. Then, 5 μL of development reagent was added, and the mixture was incubated for 2 h at room temperature before 5 μL of stop solution was added. Fluorescence signal ratio of 445 nm (Coumarin)/ 520 nm (Fluorescein) was examined on an EnVision Multilabel Reader (PerkinElmer, Inc.). The data were analyzed using Graphpad Prism5 (Graphpad Software, Inc.). The data were the mean value of three experiments.

Cell lines

SH-SY5Y cells were obtained from Shanghai Cell Bank (Type Culture Collection (TCC), Chinese Academy of Sciences) and cultured in a 1:1 mixture of MEM (01-040-1 A, BI) and F-12 (C11765500BT, Gibco) supplemented with 10% foetal bovine serum (04-001-1 A, BI), 1% Penicillin/Streptomycin (03-031-1B, BI), 1% Gluta-max (25030-081, Gibco), 1% sodium pyruvate (11360-070, Gibco) and 1% NEAA (11140050, life). SH-SY5Y cells were stably transfected with pRP-TrkB plasmids using Lipofectamine 2000 (11668019, Invitrogen) according to the manufacturer's protocol. SH-SY5Y-TrkB stable cell lines were selected in the mixed medium added with 0.5 μg/ml Puromycin (HY-B1743, MedChemExpress).

Agents

Primary antibodies against TrkB (4603), PLC-γ (5690), phosphor-PLC-γ (14008), Erk1/2 (4695), phosphor-Erk1/2 (4370), phosphor-Akt (13038, 4060), GAPDH (2118) and anti-rabbit or anti-mouse IgG horseradish peroxidase (HRP)-linked secondary antibodies were purchased from Cell Signaling Technology (Boston, MA, USA). Primary antibodies against Akt (SC8312), phosphor-TrkB (SC-135645), were purchased from Santa Cruz Biotechnology (Santa Cruz, CA, USA). Larotrectinib (LOXO-101) were purchased from the Selleckchem Company (Houston, TX, USA). These compounds were dissolved in DMSO (Sigma-Aldrich, St. Louis, MO, USA) at a concentration of 10 mmol/L and the solution was stored at -20 □.

Western blot analysis (WB)

Cells were treated with various concentrations of **9o** with or without BDNF (10 ng/ml) for a fixed time. Then cells were lysed using 1 X SDS sample lysis buffer (CST recommended) with protease and phosphatase inhibitors. Cell lysates were loaded and electrophoresed onto 8–12% SDS-PAGE gel, and then the separated proteins were transferred to a PVDF film. The film was blocked with 5% BSA (Sigma-Aldrich, St. Louis, MO, USA) in TBS solution containing 0.5% Tween-20 for 4 h at room temperature, then incubated with corresponding primary antibody (1:1000–1:200) overnight at 4 □. After washing with TBST, HRP-conjugated secondary antibody was incubated for 2 h. The protein signals were visualized by ECL Western Blotting Detection Kit (Thermo Scientific, Grand Island, NY, USA), and detected with Amersham Imager 600 system (GE, Boston, MA, USA).

Anti-proliferation assay in vitro

Cells were placed in 96-well plates (1500-3000/well) in complete medium. After incubation overnight, the cells were exposed to various concentrations (0.000457~ 3 μM) of compounds with or

without BDNF (10 ng/ml) for further 72 h. Cell proliferation was evaluated by Cell Counting Kit 8 (CCK8, CK04, Dojindo Laboratories, Kumamoto, Japan). IC_{50} values were calculated by concentration-response curve fitting using GraphPad Prism 5.0 software. Each IC_{50} value is expressed as mean ± SD.

Wound healing, migration and invasion assay

Cells (2 X 10^6/well) were seeded in a 6 well plate and allowed to grow to nearly 100% confluence in a culture medium. Subsequently, a cell free line was manually created by scratching the confluent cell monolayers with a 200 μL pipette tip. The wounded cell monolayers were washed three times with PBS and incubated in mixed medium of MEM and F-12 (containing 2% FBS) with or without BDNF at a concentration of 10 ng/mL and different concentrations of **9o** for 24 h. Three scratched fields were randomly chosen and the images were captured by a bright field microscope (CKX41; Olympus). The percentage of wound closure was measured using Adobe Photoshop 7.0.1 (Adobe Systems Inc., San Jose, CA). The experiment was performed three times, each in triplicate.

Cell migration assays were evaluated in Transwell chambers (Corning Costar). Cell invasion assays were evaluated in Magrigel invasion chambers (Corning Costar). 1.5 X 10^6 tumor cells in 200 μL FBS free medium of different doses of test compound (0, 8, 40, 200 nM) were plated in the top chamber, 800 μL complete medium with or without BDNF (10 ng/mL) was added to the bottom chamber. After incubation for 24 h at 37 □, the cells were fixed in 100% methanol and stained with 0.25% crystal violet; the cells that had not migrated from the top surface of the filters were removed with cotton. Migrated cells were quantitated by counting cells in six randomly selected fields on each filter under a microscope at 200X magnification and graphed as the mean of three independent experiments.

Acknowledgements

The authors appreciate the financial support from National Natural Science Foundation of China (81820108029, 21572230, 81874285, 81673285, 81425021 and 31800638), Key Laboratory of Precision Chemical Drug Development (201805010007), Natural Science Foundation of Guangdong Province (2018A030313003, 2015A030312014, 2015A030306042 and 2016A050502041 and Jinan University for their financial support.

Abbreviations

Trk, tropomyosin receptor kinases; IC_{50}, half-maximal (50%) inhibitory concentration of a substance; Abl, Abelson tyrosine kinase; BDNF, brain-derived neurotrophic factor; NGF, nerve growth factor;

NT-4, Neurotrophin-4; NT-3, Neurotrophin-3; Ras, rat sarcoma protein; Erk, extracellular regulated protein kinases; PI3K, phosphoinositide 3-kinases; Akt, protein kinase B; PLC-γ, phospholipase C isotype γ; PKC, protein kinase C; NB, neuroblastoma; FDA, Food and Drug Administration; ROS1, proto-oncogene tyrosine-protein kinase 1; ALK, anaplastic lymphoma kinase; ER, endoplasmic reticulum; Bcr, breakpoint cluster region protein; MeOH, methanol; $PdCl_2(PPh_3)_2$, Bis(triphenylphosphine)palladium(II) chloride; Et_3N, triethylamine; MeCN, acetonitrile; rt, room temperature; DIPEA, N,N-Diisopropylethylamine; DMF, N,N-Dimethylformamide; t-BuOK, potassium tert-butoxide; THF, tetrahydrofuran; LiOH, Lithium hydroxide; HATU, 1-[Bis(dimethylamino)methylene]-1H-1,2,3-triazolo[4,5-b]pyridinium 3-oxid hexafluorophosphate; CF_3COOH, trifluoroacetic acid; DCM, dichloromethane; DFG, Asp-Phe-Gly; SAR, structure activity relationship; ATP, Adenosine Triphosphate; SDS-PAGE, sodium dodecyl sulfate-polyacrylamide gel electrophoresis; GAPDH, glyceraldehyde 3-phosphate dehydrogenase; BBB, blood-brain-barrier; TLC, thin-layer chromatography; NMR, nuclear magnetic resonance; TMS, tetramethylsilane; ESI-MS, electrospray ionization mass spectrometry; HPLC, high-performance liquid chromatography; LC-MS, liquid chromatography–mass spectrometry; HRMS, high-resolution mass spectrometry; DMSO, dimethylsulfoxide; Tris, tris(hydroxymethyl)aminomethane; DTT, dithiothreitol; MES, 2-(N-morpholino)ethanesulfonic acid; PEG, polyethylene glycol; FRET, fluorescence resonance energy transfer; HEPES, 4-(2-hydroxyethyl)-1-piperazineethanesulfonic acid; EGTA, ethylene glycol-bis(β -aminoethyl ether)-N,N,N',N'-tetraacetic acid; MEM, minimum essential medium; NEAA, non-essential amino acids; PVDF, polyvinylidene fluoride; BSA, albumin from bovine serum; TBS, tris buffered saline. HRP, horseradish peroxidase; FBS, fetal bovine serum.

References

[1] E.J. Huang, L.F. Reichardt. Trk receptors: Roles in neuronal signal transduction. *Annu. Rev. Biochem.* 72 (2003) 609-642. https://doi.org/10.1146/annurev.biochem.72.121801.161629.

[2] S.D. Skaper. The neurotrophin family of neurotrophic factors: an overview. *Methods in molecular biology (Clifton, N.J.)* 846 (2012) 1-12. https://doi.org/10.1007/978-1-61779-536-7_1.

[3] K. Deinhardt, M.V. Chao. Trk receptors. *Handb. Exp. Pharmacol.* 220 (2014) 103-19. https://doi.org/10.1007/978-3-642-45106-5_5.

[4] R.J. Smeyne, R. Klein, A. Schnapp, L.K. Long, S. Bryant, A. Lewin, S.A. Lira, M. Barbacid. Severe sensory and sympathetic neuropathies in mice carrying a disrupted Trk/NGF receptor gene.

Nature 368 (1994) 246-9. https://doi.org/10.1038/368246a0.

[5] E.K. Lucas, A. Jegarl, R.L. Clem. Mice lacking TrkB in parvalbumin-positive cells exhibit sexually dimorphic behavioral phenotypes. *Behavioural Brain Research* 274 (2014) 219-225. https://doi.org/10.1016/j.bbr.2014.08.011.

[6] M.A. Kahn, S. Kumar, D. Liebl, R. Chang, L.F. Parada, J. De Vellis. Mice lacking NT-3, and its receptor TrkC, exhibit profound deficiencies in CNS glial cells. *Glia* 26 (1999) 153-65. https://doi.org/10.1002/(sici)1098-1136(199904)26:2<153::Aid-glia6>3.3.Co;2-q.

[7] A. Vaishnavi, A.T. Le, R.C. Doebele. TRKing Down an Old Oncogene in a New Era of Targeted Therapy. *Cancer Discov.* 5 (2015) 25-34. https://doi.org/10.1158/2159-8290.cd-14-0765.

[8] A.M. Lange, H.-W. Lo. Inhibiting TRK Proteins in Clinical Cancer Therapy. *Cancers* 10 (2018) 105-119. https://doi.org/10.3390/cancers10040105.

[9] Y. Chen, S.H. Tseng. Targeting tropomyosin-receptor kinase fused gene in cancer. *Anticancer Res.* 34 (2014) 1595-600.

[10] R. Bagatell, S.L. Cohn. Genetic discoveries and treatment advances in neuroblastoma. *Curr. Opin. Pediatr.* 28 (2016) 19-25. https://doi.org/10.1097/mop.0000000000000296.

[11] Y. Cao, Y. Jin, J. Yu, J. Wang, J. Yan, Q.J.O. Zhao. Research progress of neuroblastoma related gene variations. *Oncotarget* 8 (2017) 18444. https://doi.org/10.18632/oncotarget.14408.

[12] G.M. Brodeur, J.E. Minturn, R. Ho, A.M. Simpson, R. Iyer, C.R. Varela, J.E. Light, V. Kolla, A.E. Evans. Trk receptor expression and inhibition in neuroblastomas. *Clin. Cancer Res.* 15 (2009) 3244-50. https://doi.org/10.1158/1078-0432.Ccr-08-1815.

[13] A. Schramm, J.H. Schulte, K. Astrahantseff, O. Apostolov, V. van Limpt, H. Sieverts, S. Kuhfittig-Kulle, P. Pfeiffer, R. Versteeg, A. Eggert. Biological effects of TrkA and TrkB receptor signaling in neuroblastoma. *Cancer lett.* 228 (2005) 143-153. https://doi.org/10.1016/j.canlet.2005.02.051.

[14] S. Aveic, M. Pantile, A. Seydel, M.R. Esposito, C. Zanon, G. Li, G.P. Tonini. Combating autophagy is a strategy to increase cytotoxic effects of novel ALK inhibitor entrectinib in neuroblastoma cells. *Oncotarget* 7 (2016) 5646-5663. https://doi.org/10.18632/oncotarget.6778.

[15] P.E. Zage, T.C. Graham, L. Zeng, W. Fang, C. Pien, K. Thress, C. Omer, J.L. Brown, P.A. Zweidler-McKay. The selective Trk inhibitor AZ623 inhibits brain-derived neurotrophic factor-mediated neuroblastoma cell proliferation and signaling and is synergistic with topotecan.

Cancer 117 (2011) 1321-91. https://doi.org/10.1002/cncr.25674.

[16] R. Iyer, L. Wehrmann, R.L. Golden, K. Naraparaju, J.L. Croucher, S.P. MacFarland, P. Guan, V. Kolla, G. Wei, N. Cam, G. Li, Z. Hornby, G.M. Brodeur. Entrectinib is a potent inhibitor of Trk-driven neuroblastomas in a xenograft mouse model. *Cancer lett.* 372 (2016) 179-86. https://doi.org/10.1016/j.canlet.2016.01.018.

[17] A. Eggert, M.A. Grotzer, N. Ikegaki, X.G. Liu, A.E. Evans, G.M. Brodeur. Expression of the neurotrophin receptor TrkA down-regulates expression and function of angiogenic stimulators in SH-SY5Y neuroblastoma cells. *Cancer Res.* 62 (2002) 1802-1808.

[18] R. Ho, A. Eggert, T. Hishiki, J.E. Minturn, N. Ikegaki, P. Foster, A.M. Camoratto, A.E. Evans, G.M. Brodeur. Resistance to chemotherapy mediated by TrkB in neuroblastomas. *Cancer Res.* 62 (2002) 6462-6466.

[19] J. Zou, Z. Zhang, F. Xu, S. Cui, C. Qi, J. Luo, Z. Wang, X. Lu, Z. Tu, X. Ren, L. Song, K. Ding. GZD2202, a novel TrkB inhibitor, suppresses BDNF-mediated proliferation and metastasis in neuroblastoma models. *J. Drug Target.* (2018) 1-9. https://doi.org/10.1080/1061186x.2018.1533964.

[20] W. Yan, N.R. Lakkaniga, F. Carlomagno, M. Santoro, N.Q. McDonald, F. Lv, N. Gunaganti, B. Frett, H.-y. Li. Insights into Current Tropomyosin Receptor Kinase (TRK) Inhibitors: Development and Clinical Application. *J. Med. Chem.* (2018). https://doi.org/10.1021/acs.jmedchem.8b01092.

[21] C. McCarthy, E. Walker. Tropomyosin receptor kinase inhibitors: a patent update 2009-2013. *Expert Opin. Ther. Pat.* 24 (2014) 731-744. https://doi.org/10.1517/13543776.2014.910195.

[22] J.J. Bailey, R. Schirrmacher, K. Farrell, V. Bernard-Gauthier. Tropomyosin receptor kinase inhibitors: an updated patent review for 2010-2016-Part I. *Expert Opin. Ther. Pat.* 27 (2017) 733-751. https://doi.org/10.1080/13543776.2017.1297796.

[23] J.J. Bailey, R. Schirrmacher, K. Farrell, V. Bernard-Gauthier. Tropomyosin receptor kinase inhibitors: an updated patent review for 2010-2016-Part II. *Expert Opin. Ther. Pat.* 27 (2017) 831-849. https://doi.org/10.1080/13543776.2017.1297797.

[24] A. Drilon, T.W. Laetsch, S. Kummar, S.G. DuBois, U.N. Lassen, G.D. Demetri, M. Nathenson, R.C. Doebele, A.F. Farago, A.S. Pappo, B. Turpin, A. Dowlati, M.S. Brose, L. Mascarenhas, N. Federman, J. Berlin, W.S. El-Deiry, C. Baik, J. Deeken, V. Boni, R. Nagasubramanian, M. Taylor, E.R. Rudzinski, F. Meric-Bernstam, D.P.S. Sohal, P.C. Ma, L.E. Raez, J.F. Hechtman, R. Benayed, M. Ladanyi, B.B. Tuch, K. Ebata, S. Cruickshank, N.C. Ku, M.C. Cox, D.S. Hawkins, D.S. Hong, D.M.

Hyman. Efficacy of Larotrectinib in TRK Fusion-Positive Cancers in Adults and Children. *N. Engl. J. Med.* 378 (2018) 731-739. https://doi.org/10.1056/NEJMoa1714448.

[25] R.C. Doebele, L.E. Davis, A. Vaishnavi, A.T. Le, A. Estrada-Bernal, S. Keysar, A. Jimeno, M. Varella-Garcia, D.L. Aisner, Y. Li, J. Stephens, D. Morosini, B.B. Tuch, M. Fernandes, N. Nanda, J.A. Low. An Oncogenic NTRK Fusion in a Patient with Soft-Tissue Sarcoma with Response to the Tropomyosin-Related Kinase Inhibitor LOXO-101. *Cancer Discov.* 5 (2015) 1049-1057. https://doi.org/10.1158/2159-8290.Cd-15-0443.

[26] T.W. Laetsch, S.G. DuBois, L. Mascarenhas, B. Turpin, N. Federman, C.M. Albert, R. Nagasubramanian, J.L. Davis, E. Rudzinski, A.M. Feraco, B.B. Tuch, K.T. Ebata, M. Reynolds, S. Smith, S. Cruickshank, M.C. Cox, A.S. Pappo, D.S. Hawkins. Larotrectinib for paediatric solid tumours harbouring NTRK gene fusions: phase 1 results from a multicentre, open-label, phase 1/2 study. *Lancet Oncol.* 19 (2018) 705-714. https://doi.org/10.1016/s1470-2045(18)30119-0.

[27] A.F. Farago, L.P. Le, Z. Zheng, A. Muzikansky, A. Drilon, M. Patel, T.M. Bauer, S.V. Liu, S.-H.I. Ou, D. Jackman, D.B. Costa, P.S. Multani, G.G. Li, Z. Hornby, E. Chow-Maneval, D. Luo, J.E. Lim, A.J. Iafrate, A.T. Shaw. Durable Clinical Response to Entrectinib in NTRK1-Rearranged Non-Small Cell Lung Cancer. *J. Thorac. Oncol.* 10 (2015) 1670-1674. https://doi.org/10.1097/01.JTO.0000473485.38553.f0.

[28] E. Ardini, M. Menichincheri, P. Banfi, R. Bosotti, C. De Ponti, R. Pulci, D. Ballinari, M. Ciomei, G. Texido, A. Degrassi, N. Avanzi, N. Amboldi, M.B. Saccardo, D. Casero, P. Orsini, T. Bandiera, L. Mologni, D. Anderson, G. Wei, J. Harris, J.-M. Vernier, G. Li, E. Felder, D. Donati, A. Isacchi, E. Pesenti, P. Magnaghi, A. Galvani. Entrectinib, a Pan-TRK, ROS1, and ALK Inhibitor with Activity in Multiple Molecularly Defined Cancer Indications. *Mol. Cancer Ther.* 15 (2016) 628-639. https://doi.org/10.1158/1535-7163.Mct-15-0758.

[29] M. Menichincheri, E. Ardini, P. Magnaghi, N. Avanzi, P. Banfi, R. Bossi, L. Buffa, G. Canevari, L. Ceriani, M. Colombo, L. Corti, D. Donati, M. Fasolini, E. Felder, C. Fiorelli, F. Fiorentini, A. Galvani, A. Isacchi, A.L. Borgia, C. Marchionni, M. Nesi, C. Orrenius, A. Panzeri, E. Pesenti, L. Rusconi, M.B. Saccardo, E. Vanotti, E. Perrone, P. Orsini. Discovery of Entrectinib: A New 3-Aminoindazole As a Potent Anaplastic Lymphoma Kinase (ALK), c-ros Oncogene 1 Kinase (ROS1), and Pan-Tropomyosin Receptor Kinases (Pan-TRKs) inhibitor. *J. Med. Chem.* 59 (2016) 3392-3408. https://doi.org/10.1021/acs.jmedchem.6b00064.

[30] A. Drilon, S. Siena, S.-H.I. Ou, M. Patel, M.J. Ahn, J. Lee, T.M. Bauer, A.F. Farago, J.J. Wheler, S.V. Liu, R. Doebele, L. Giannetta, G. Cerea, G. Marrapese, M. Schirru, A. Amatu, K. Bencardino, L. Palmeri, A. Sartore-Bianchi, A. Vanzulli, S. Cresta, S. Damian, M. Duca, E. Ardini, G. Li, J. Christiansen, K. Kowalski, A.D. Johnson, R. Patel, D. Luo, E. Chow-Maneval, Z. Hornby, P.S. Multani, A.T. Shaw, F.G. De Braud. Safety and Antitumor Activity of the Multitargeted Pan-TRK, ROS1, and ALK Inhibitor Entrectinib: Combined Results from Two Phase I Trials (ALKA-372-001 and STARTRK-1). *Cancer Discov.* 7 (2017) 400-409. https://doi.org/10.1158/2159-8290.Cd-16-1237.

[31] V. Bernard-Gauthier, J.J. Bailey, A.V. Mossine, S. Lindner, L. Vomacka, A. Aliaga, X. Shao, C.A. Quesada, P. Sherman, A. Mahringer, A. Kostikov, M. Grand'Maison, P. Rosa-Neto, J.-P. Soucy, A. Thiel, D.R. Kaplan, G. Fricker, B. Wängler, P. Bartenstein, R. Schirrmacher, P.J.H. Scott. A Kinome-Wide Selective Radiolabeled TrkB/C Inhibitor for in Vitro and in Vivo Neuroimaging: Synthesis, Preclinical Evaluation, and First-in-Human. *J. Med. Chem.* 60 (2017) 6897-6910. https://doi.org/10.1021/acs.jmedchem.7b00396.

[32] V. Bernard-Gauthier, A.V. Mossine, A. Mahringer, A. Aliaga, J.J. Bailey, X. Shao, J. Stauff, J. Arteaga, P. Sherman, M. Grand'Maison, P.-L. Rochon, B. Wängler, C. Wängler, P. Bartenstein, A. Kostikov, D.R. Kaplan, G. Fricker, P. Rosa-Neto, P.J.H. Scott, R. Schirrmacher. Identification of [18F]TRACK, a Fluorine-18-Labeled Tropomyosin Receptor Kinase (Trk) Inhibitor for PET Imaging. *J. Med. Chem.* 61 (2018) 1737-1743. https://doi.org/10.1021/acs.jmedchem.7b01607.

[33] F.M. Yakes, J. Chen, J. Tan, K. Yamaguchi, Y. Shi, P. Yu, F. Qian, F. Chu, F. Bentzien, B. Cancilla, J. Orf, A. You, A.D. Laird, S. Engst, L. Lee, J. Lesch, Y.-C. Chou, A.H. Joly. Cabozantinib (XL184), a Novel MET and VEGFR2 Inhibitor, Simultaneously Suppresses Metastasis, Angiogenesis, and Tumor Growth. *Mol. Cancer Ther.* 10 (2011) 2298-2308. https://doi.org/10.1158/1535-7163.Mct-11-0264.

[34] P.P. Patwardhan, K.S. Ivy, E. Musi, E. de Stanchina, G.K. Schwartz. Significant blockade of multiple receptor tyrosine kinases by MGCD516 (Sitravatinib), a novel small molecule inhibitor, shows potent anti-tumor activity in preclinical models of sarcoma. *Oncotarget* 7 (2016) 4093-4109. https://doi.org/10.18632/oncotarget.6547.

[35] B.D. Smith, M.D. Kaufman, C.B. Leary, B.A. Turner, S.C. Wise, Y.M. Ahn, R.J. Booth, T.M. Caldwell, C.L. Ensinger, M.M. Hood, W.-P. Lu, T.W. Patt, W.C. Patt, T.J. Rutkoski, T. Samarakoon, H. Telikepalli, L. Vogeti, S. Vogeti, K.M. Yates, L. Chun, L.J. Stewart, M. Clare, D.L. Flynn. Altiratinib Inhibits Tumor Growth, Invasion, Angiogenesis, and Microenvironment-Mediated Drug Resistance via

Balanced Inhibition of MET, TIE2, and VEGFR2. *Mol. Cancer Ther.* 14 (2015) 2023-2034. https://doi.org/10.1158/1535-7163.Mct-14-1105.

[36] B.D. Smith, C.B. Leary, B.A. Turner, M.D. Kaufman, S.C. Wise, M.E.R. Garcia-Rendueles, J.A. Fagin, D.L. Flynn. Altiratinib is a potent inhibitor of TRK kinases and is efficacious in TRK-fusion driven cancer models. *Cancer Res.* 75 (2015). https://doi.org/10.1158/1538-7445.Am2015-790.

[37] M. Russo, S. Misale, G. Crisafulli, G. Corti, G. Rospo, L. Novara, B. Mussolin, A. Bartolini, G. Wei, N. Cam, R. Patel, S. Yan, R. Shoemaker, R. Wild, G. Li, G. Siravegna, L. Lazzari, N.F. Di, A. Bardelli, A.S. Bianchi, S. Siena. Acquired Resistance to the TRK Inhibitor Entrectinib in Colorectal Cancer. *Cancer Discov* 6 (2016) 36-44.

[38] A. Drilon, G. Li, S. Dogan, M. Gounder, R. Shen, M. Arcila, L. Wang, D.M. Hyman, J. Hechtman, G. Wei, N.R. Cam, J. Christiansen, D. Luo, E.C. Maneval, T. Bauer, M. Patel, S.V. Liu, S.H.I. Ou, A. Farago, A. Shaw, R.F. Shoemaker, J. Lim, Z. Hornby, P. Multani, M. Ladanyi, M. Berger, N. Katabi, R. Ghossein, A.L. Ho. What hides behind the MASC: clinical response and acquired resistance to entrectinib after ETV6-NTRK3 identification in a mammary analogue secretory carcinoma (MASC). *Annals of Oncology* 27 (2016) 920-926. https://doi.org/10.1093/annonc/mdw042.

[39] X. Ren, X. Pan, Z. Zhang, D. Wang, X. Lu, Y. Li, D. Wen, H. Long, J. Luo, Y. Feng, X. Zhuang, F. Zhang, J. Liu, F. Leng, X. Lang, Y. Bai, M. She, Z. Tu, J. Pan, K. Ding. Identification of GZD824 as an Orally Bioavailable Inhibitor That Targets Phosphorylated and Nonphosphorylated Breakpoint Cluster Region–Abelson (Bcr-Abl) Kinase and Overcomes Clinically Acquired Mutation-Induced Resistance against Imatinib. *J. Med. Chem.* 56 (2013) 879-894. https://doi.org/10.1021/jm301581y.

[40] R. Kerkela, L. Grazette, R. Yacobi, C. Iliescu, R. Patten, C. Beahm, B. Walters, S. Shevtsov, S. Pesant, F.J. Clubb, A. Rosenzweig, R.N. Salomon, R.A. Van Etten, J. Alroy, J.-B. Durand, T. Force. Cardiotoxicity of the cancer therapeutic agent imatinib mesylate. *Nat. Med.* 12 (2006) 908-916. https://doi.org/10.1038/nm1446.

[41] T. Force, D.S. Krause, R.A. Van Etten. Molecular mechanisms of cardiotoxicity of tyrosine kinase inhibition. *Nat. Rev. Cancer* 7 (2007) 332-344. https://doi.org/10.1038/nrc2106.

[42] R. Chinchilla, C. Najera. The sonogashira reaction: A booming methodology in synthetic organic chemistry. *Chem. Rev.* 107 (2007) 874-922. https://doi.org/10.1021/cr050992x.

[43] Z. Wang, H. Bian, S.G. Bartual, W. Du, J. Luo, H. Zhao, S. Zhang, C. Mo, Y. Zhou, Y. Xu, Z. Tu, X. Ren, X. Lu, R.A. Brekken, L. Yao, A.N. Bullock, J. Su, K. Ding. Structure-Based Design of

Tetrahydroisoquinoline-7-carboxamides as Selective Discoidin Domain Receptor 1 (DDR1) Inhibitors. *J. Med. Chem.* 59 (2016) 5911-5916. https://doi.org/10.1021/acs.jmedchem.6b00140.

[44] S.M. Rodems, B.D. Hamman, C. Lin, J. Zhao, S. Shah, D. Heidary, L. Makings, J.H. Stack, B.A. Pollok. A FRET-based assay platform for ultra-high density drug screening of protein kinases and phosphatases. *Assay Drug Dev. Technol.* 1 (2002) 9-19. https://doi.org/10.1089/154065802761001266.

[45] L.G. Rodriguez, X. Wu, J.-L. Guan. Wound-healing assay. *Methods in molecular biology (Clifton, N.J.)* 294 (2005) 23-9.

[46] Z. Otwinowski, W. Minor. Processing of X-ray diffraction data collected in oscillation mode. *Methods Enzymol.* 276 (1997) 307-326. https://doi.org/10.1016/s0076-6879(97)76066-x.

[47] A.J. McCoy, R.W. Grosse-Kunstleve, P.D. Adams, M.D. Winn, L.C. Storoni, R.J. Read. Phaser crystallographic software. *J. Appl. Crystallogr.* 40 (2007) 658-674. https://doi.org/10.1107/s0021889807021206.

[48] P. Emsley, K. Cowtan. Coot: model-building tools for molecular graphics. *Acta Crystallogr. Sect. D-Struct. Biol.* 60 (2004) 2126-2132. https://doi.org/10.1107/s0907444904019158.

[49] P.D. Adams, P.V. Afonine, G. Bunkoczi, V.B. Chen, N. Echols, J.J. Headd, L.-W. Hung, S. Jain, G.J. Kapral, R.W.G. Kunstleve, A.J. McCoy, N.W. Moriarty, R.D. Oeffner, R.J. Read, D.C. Richardson, J.S. Richardson, T.C. Terwilliger, P.H. Zwart. The Phenix software for automated determination of macromolecular structures. *Methods* 55 (2011) 94-106. https://doi.org/10.1016/j.ymeth.2011.07.005.

1. 3-(Imidazo[1,2-a]pyrazin-3-ylethynyl)-2-methylbenzamides as selective Trk inhibitors.
2. **9o** suppressed TrkA/B/C with IC_{50} values of 2.65, 10.47 and 2.95 nM, respectively and inhibited the proliferation of SH-SY5Y-TrkB cells with an IC_{50} value of 58 nM.